


## Tunneling time in $\mathcal{PT}$ -symmetric systems

Peng Guo <sup>1,\*</sup>, Vladimir Gasparian <sup>1,†</sup>, Esther Jódar <sup>2,‡</sup> and Christopher Wisehart <sup>1,§</sup>

<sup>1</sup>*Department of Physics and Engineering, California State University, Bakersfield, California 93311, USA*

<sup>2</sup>*Departamento de Física Aplicada, Universidad Politécnica de Cartagena, E-30202 Murcia, Spain*



(Received 30 August 2022; accepted 1 March 2023; published 13 March 2023)

In the present work, we propose a generalization of tunneling time in parity and time ( $\mathcal{PT}$ )-symmetric systems. The properties of tunneling time in  $\mathcal{PT}$ -symmetric systems are studied with a simple contact interaction periodic finite-size diatomic  $\mathcal{PT}$ -symmetric model. The physical meaning of negative tunneling time in  $\mathcal{PT}$ -symmetric systems and its relation to spectral singularities is discussed.

DOI: [10.1103/PhysRevA.107.032210](https://doi.org/10.1103/PhysRevA.107.032210)

### I. INTRODUCTION

In standard (Hermitian) quantum mechanics, the calculation of the time interval during which a particle interacts with a barrier of arbitrary shape is not new and has attracted a great deal of interest lately. A wide variety of theoretical and experimental work on this topic has been carried out during the past two decades. This particular interest is due to the introduction of non-Hermitian elements into the Hamiltonian enabling the solution of specific problems in which, for example, a complex index of refraction is used (optics), or complex potentials are introduced far away from the interaction region of the particles [1]. The tunneling time problem was studied both theoretically and experimentally (see, e.g., Refs. [2–4] and references therein), especially in nanostructures or in mesoscopic systems smaller than 10 nm. In these systems, the tunneling time will eventually play an important role in determining transport properties, for example in the frequency-dependent conductivity response of mesoscopic conductors [5] and in the phenomenon of an adiabatic charge transport [6,7]. Several authors have studied the problem of tunneling time in passive scattering systems using a number of completely different approaches, including the oscillatory amplitude of the incident amplitude [8–11], the time-modulated barrier [12], as well as the wave-packet approach; see, e.g., Refs. [13–15]. In most approaches to the tunneling time problem, more than one tunneling-time component is involved, regardless of whether we deal with the so-called Büttiker-Landauer approach [16], the Feynman path-integral approach [17], or complex characteristic times [18–20]. Furthermore, this does not seem to be a peculiarity of quantum-mechanical waves, but rather a general result and valid not only for electrons but also for any waves (sound and electromagnetic) when their propagation through a medium is described by a differential equation of second order. For

electromagnetic waves, in Ref. [21] in the Faraday rotation scheme, it was shown that the characteristic time associated with the interaction of the classical electromagnetic wave with a finite region is a complex quantity. As a consequence, the emerging electromagnetic wave is elliptically polarized, and the major axis of the ellipse is rotated relative to the original direction of polarization. In addition, one of the components of the complex time is closely related not only to the total density of states (DOS), but also to its decomposition into partial DOS [4,16]. Furthermore, the two components are not entirely independent quantities and are connected by Kramers-Kronig relations [22]. In Ref. [23], the tunneling times associated with frustrated total internal reflection of light were investigated experimentally. It is shown that the two characteristic times correspond, respectively, to the spatial and angular shifts of the beam. Despite the progress that has been made towards understanding the longstanding problem of tunneling time in traditional quantum mechanics, as far as we know such discussions are rather scarce in non-Hermitian systems (see, e.g., Refs. [24–26]).

Without pretending to give an exhaustive overview of the possible applications of non-Hermitian systems as an ideal platform for exploring the functionality of new possible devices, we briefly present some achievements in condensed-matter physics [27], electronic circuits [28], coupled mechanical oscillators [29–31], mesoscopic superconducting wires [32], and photonic applications [33].

Most of the studies in non-Hermitian systems, both theoretical and experimental, have been carried out in parity and time ( $\mathcal{PT}$ )-symmetric systems, supporting the real spectrum of eigenvalues. In such a system, a great deal of attention was paid to the optical setups or theoretical models with the gain (through optical or electrical pumping or nonlinear interactions) and loss (due to absorption or radiation) where the properties of the  $\mathcal{PT}$ -symmetric system, including unidirectional invisibility [34–36] and double refraction [37], can be measured directly or calculated analytically. In Ref. [38] the instabilities and the possibility of establishing localized complex defect modes, with spectra lying within the allowed band, have been investigated both theoretically and experimentally. An interesting feature of resonance, as in discrete as well as

\*pguo@csub.edu

†vgasparyan@csub.edu

‡esther.jferrandez@upct.es

§cwisehart@csub.edu

scattering spectra in a  $\mathcal{PT}$ -symmetric open quantum system, was studied in Ref. [39] using the tight-binding model.

After this brief enumeration of the intriguing features of  $\mathcal{PT}$ -symmetric systems, the need for further research on the problem of tunneling time in  $\mathcal{PT}$ -symmetric systems becomes apparent. Moreover, as shown in Ref. [40], the absorbing part of the Green's function of non-Hermitian systems is no longer related to the density of states, and it is generally a complex function. Only in special cases, such as  $\mathcal{PT}$ -symmetric systems, can the absorbing part of the Green's function remain real, although a positive-definite norm is not guaranteed. The purpose of the present work goes in this direction in the sense that the concept of generalized tunneling time in  $\mathcal{PT}$ -symmetric systems is proposed. The properties of tunneling time in  $\mathcal{PT}$ -symmetric systems are studied with a simple contact interaction periodic finite-size diatomic  $\mathcal{PT}$ -symmetric model. We stress that unlike the positive-definite tunneling time  $\tau_1$  [see below, Eq. (1)] in real potential scattering theory, the  $\tau_1$  in  $\mathcal{PT}$ -symmetric systems can be either positively or negatively valued. The value of  $\tau_1$  turning negative is closely related to the motion of pole singularities of scattering amplitudes in a complex energy plane. The physical interpretation of negative valued  $\tau_1$  is also discussed.

The paper is organized as follows. The generalized tunneling time for  $\mathcal{PT}$ -symmetric systems is introduced and defined in Sec. II. A simple model and its analytic solutions are summarized in Sec. III. The averaged tunneling time per unit cell and its limit in an infinite periodic system are discussed in Sec. IV. The impact of spectral singularities and numerics is shown in Sec. V, followed by the discussion and a summary in Sec. VI.

## II. GENERALIZED TUNNELING TIME IN $\mathcal{PT}$ -SYMMETRIC SYSTEMS

In the real potential scattering theory, the concept of tunneling or delay time for a particle tunneling through potential barriers is conventionally defined through integrated density of states, which is proportional to the imaginary part of the full Green's function of systems (see, e.g., Refs. [18–20]),

$$\tau_1(E) = -\text{Im} \left[ \int_{-l}^l dx \langle x | \hat{G}(E) | x \rangle \right] \propto \int_{-l}^l dx |\langle x | \Psi_E \rangle|^2, \quad (1)$$

where  $l$  is the half-length of a potential barrier. The  $\hat{G}(E) = \frac{1}{E - \hat{H}}$  is the Green's function operator of the system. It is related to the eigenstate of the system by the spectral representation of the Green's function,

$$\hat{G}(E) = \sum_i \frac{|\Psi_{E_i}\rangle\langle\Psi_{E_i}|}{E - E_i}, \quad (2)$$

where eigenstate  $|\Psi_{E_i}\rangle$  satisfies the Schrödinger equation,

$$\hat{H}|\Psi_{E_i}\rangle = E_i|\Psi_{E_i}\rangle. \quad (3)$$

In the case of complex potential scattering theory, now one is facing the challenge of how the concept of tunneling time should be generalized and defined properly. One of the key elements in developing the concept of tunneling or

delay time in a real potential scattering theory is counting the probability that a particle spends inside of a barrier; see, e.g., Refs. [41–43]. However, in complex potential scattering theory, the norm of states is no longer conserved, so the probability interpretation of the tunneling time becomes problematic. In addition, the spectral representation of the Green's function now depends on the eigenstates of both  $\hat{H}$  and its adjoint  $\hat{H}^\dagger$ ,

$$\hat{G}(E) = \sum_i \frac{|\Psi_{E_i}\rangle\langle\tilde{\Psi}_{E_i}|}{E - E_i}, \quad (4)$$

where

$$\hat{H}^\dagger|\tilde{\Psi}_{E_i}\rangle = E_i|\tilde{\Psi}_{E_i}\rangle. \quad (5)$$

The biorthogonal and normalization relations can only be established by eigenstates of dual systems together [24,44,45],

$$\sum_i |\Psi_{E_i}\rangle\langle\tilde{\Psi}_{E_i}| = \mathbb{I}. \quad (6)$$

Hence, the discontinuity of the Green's function crossing the branch cut in the complex  $E$ -plane is in general a complex function, and it is no longer equivalent to the imaginary part of the Green's function; see Ref. [40]. Its relevance to the conventional definition of the density of states is also lost,

$$\text{Disc}_E \langle x | \hat{G}(E) | x \rangle \propto \langle x | \Psi_E \rangle \langle \tilde{\Psi}_E | x \rangle \neq |\langle x | \Psi_E \rangle|^2, \quad (7)$$

where

$$\text{Disc}_E \hat{G}(E) = \frac{\hat{G}(E + i0) - \hat{G}(E - i0)}{2i}. \quad (8)$$

Fortunately, in a  $\mathcal{PT}$ -symmetric system, as shown in Ref. [40], because of symmetry constraints, the discontinuity of the Green's function is still a real function, hence it is identical to the imaginary part of the Green's function,  $\text{Disc}_E \hat{G}(E) = \text{Im} \hat{G}(E)$ . However, as a consequence of norm violation with a complex potential, positivity of the imaginary part of the Green's function is not guaranteed. In this work, the tunneling time through  $\mathcal{PT}$ -symmetric barriers is still defined by an integrated Green's function, hence most of the formalisms that are developed for real potential scattering theory can still apply directly to a  $\mathcal{PT}$ -symmetric system. The imaginary part of the Green's function is now referred to as the generalized density of states of a  $\mathcal{PT}$ -symmetric system. Following the definition in Refs. [18–20], two components of the traversal time  $\tau_E$  are introduced by

$$\tau_E = \tau_2(E) + i\tau_1(E) = - \int_{-l}^l dx \langle x | \hat{G}(E) | x \rangle, \quad (9)$$

where  $\tau_1$  and  $\tau_2$  may be interpreted as two components of the generalized concept of Büttiker-Landauer tunneling time that are connected with the generalized density of states and the Landauer resistance in a  $\mathcal{PT}$ -symmetric system. The positivity and negativity of the generalized tunneling time  $\tau_1$  simply reflect the nature of potential barriers that either tend to keep a particle in or force it out. The negative value portion of  $\tau_1$  is thus physically inaccessible and hence behaves similarly to a forbidden gap in a periodic system.

As shown in Refs. [19,20], the integrated Green's function is related to the transmission and reflection amplitudes by

$$-\int_{-l}^l dx \langle x | \hat{G}(E) | x \rangle = \frac{d}{dE} \ln[t(k)e^{ik2l}] + \frac{r^{(L)}(k) + r^{(R)}(k)}{4E} e^{ik2l}, \quad (10)$$

where  $t(k)$  and  $r^{(L/R)}(k)$  are the transmission and left/right reflection amplitudes, respectively, and  $k = \sqrt{2mE}$  is the momentum of a particle. In practice, it is more convenient to compute the tunneling time directly through the transmission and reflection amplitudes.

### III. A SIMPLE CONTACT INTERACTION $\mathcal{PT}$ -SYMMETRIC IMPURITIES MODEL

In this section, a simple contact interaction  $\mathcal{PT}$ -symmetric model is adopted to investigate the properties of tunneling time through layers of  $\mathcal{PT}$ -symmetric barriers. Each single cell of a barrier is composed of two complex components: one absorbing component with loss, and another emissive component with gain. Two components are placed symmetrically on two sides of the cell along the center; the gain and loss in each single cell are balanced. The potential barrier in a single cell hence is  $\mathcal{PT}$ -symmetric:

$$V(-x) = V^*(x). \quad (11)$$

The Hamiltonian of barriers is thus given by

$$\hat{H} = -\frac{1}{2m} \frac{d^2}{dx^2} + \sum_{n=-N}^N V(x - nL), \quad (12)$$

where  $2N + 1$  is the total number of cells, and  $L$  represents the length of a single cell. The total length of the barriers is  $2l = (2N + 1)L$ . A simple diatomic  $\mathcal{PT}$ -symmetric contact interaction potential that represents two complex-conjugate impurities is used:

$$V(x) = V\delta(x - a) + V^*\delta(x + a), \quad V = |V|e^{i\theta}. \quad (13)$$

Two complex-conjugate impurities are placed on two sides of a cell's center with equal distance  $a$ . One is absorbing with loss and another is emissive with an equal amount of gain. The physical realization of such a  $\mathcal{PT}$ -symmetric model may be accomplished in a planar slab waveguide as discussed in Ref. [46].

The simple contact interaction  $\mathcal{PT}$ -symmetric impurities model adopted in this work may be considered as a special case of the periodic diatomic contact interaction model. It turns out that the analytic form of the scattering solutions can be found in a highly nontrivial way; see, e.g., the characteristics determinant approach in Refs. [47–49]. In what follows, we will simply summarize the results of scattering solutions. A brief introduction about the general scattering theory, some useful relations, and the characteristics determinant approach are provided in Appendix A.

The transmission and left/right reflection amplitudes are given by

$$t(k) = \frac{\sec(Q(2N + 1)L)e^{-ik(2N+1)L}}{1 + i \operatorname{Im}\left[\frac{e^{-ikL}}{t_0(k)}\right] \frac{\tan(Q(2N+1)L)}{\sin(QL)}},$$

$$\frac{r^{(L/R)}(k)}{t(k)} = \left[ \frac{r_0^{(L/R)}(k)}{t_0(k)} \right] \frac{\sin(Q(2N + 1)L)}{\sin(QL)}, \quad (14)$$

where  $t_0(k)$  and  $r_0^{(L/R)}(k)$  are transmission and reflection amplitudes by a single cell ( $N = 0$ ),

$$\frac{1}{t_0(k)} = 1 + 2\frac{im|V|}{k} \cos\theta + 2i\left(\frac{m|V|}{k}\right)^2 \sin(k2a)e^{ik2a},$$

$$\frac{r_0^{(L/R)}(k)}{t_0(k)} = -2\frac{im|V|}{k} \left[ \cos(k2a \mp \theta) + \frac{m|V|}{k} \sin(k2a) \right]. \quad (15)$$

$Q$  plays the role of crystal momentum for a periodic lattice and is related to  $k$  by

$$\cos(QL) = \operatorname{Re}\left[\frac{e^{-ikL}}{t_0(k)}\right]. \quad (16)$$

It is quite remarkable to see that the transmission and reflection amplitudes for a periodic many-scatters system are all related to single-cell scattering amplitudes in a very compact fashion. If  $Q$  is treated as a free parameter that represents the collective mode of the entire lattice of all impurities, the short-range interaction dynamics that is described by single-cell scattering amplitudes and long-range physics of collective mode are totally factorized. The factorization of short-range dynamics and long-range correlation for an infinitely long periodic lattice or in a periodic finite box has been a well-known fact in both condensed-matter physics and nuclear/hadron physics. When the interaction range is much smaller than the size of a cell or a trap, the quantization conditions are given by a compact formula, in which two components—(i) the short-range particles dynamics, and (ii) the long-range geometric effect due to the periodic box or trap—are well separated. The compact form is known as the Korringa-Kohn-Rostoker (KKR) method [50,51] in condensed-matter physics, the Lüscher formula [52] in LCQD, and the Busch-Englert-Rzażewski-Wilkens (BERW) formula [53] in a harmonic-oscillator trap in the nuclear physics community. Other related useful discussions can be found in, e.g., Refs. [54–57]; see also the discussion in Appendix B. The emergence of periodic dynamics in a finite-size system may be best demonstrated by the characteristic determinant approach that was developed in Refs. [47–49]. The characteristic determinant approach may be considered as a ground-up approach. The key idea is to start from a single cell and gradually build up to a many-cell system by adding one cell at a time. Using the recursion relations satisfied by the determinant of the  $D$ -matrix,  $D = 1 - \hat{G}_0 \hat{V}$ , where  $\hat{G}_0 = \frac{1}{E - \hat{H}_0}$  is a free propagator of a particle, when the cells are periodically arranged, the scattering dynamics for a many-cell system is given by two factorized components: (i) the scattering amplitudes of a single cell that are the result of short-range interaction; and (ii) the geometric factors that are associated

with the periodic structure of the entire system, which also describe the collective modes of a finite-size crystal.

Finally, we note that the compact forms of the transmission amplitude and crystal-momentum  $Q$  in Eqs. (14) and (16) in terms of real and imaginary parts of  $\frac{e^{-ikL}}{t_0(k)}$  are only valid and defined for the real  $k$ 's. For complex  $k$ , e.g., when looking for the pole position in the complex- $k$  plane, the correct values are given by an analytic continuation of explicit expressions by inserting the analytic form of  $t_0(k)$  in Eq. (15) into Eqs. (14) and (16), assuming  $k$  is real.

#### IV. AVERAGING TUNNELING TIME PER UNIT CELL AT THE LARGE- $N$ LIMIT

As  $N$  is increased, the band structure starts to appear, and the tunneling time starts oscillating drastically due to  $\cos(Q(2N+1)L)$  and  $\sin(Q(2N+1)L)$  factors. To evaluate the asymptotic behavior of the tunneling time, it is more convenient to define the tunneling time per unit cell,

$$\hat{\tau}(k) = \frac{\tau_E}{(2N+1)L}. \quad (17)$$

For large  $N$ , the second term in Eq. (10) is suppressed and the first term is a fast oscillating term. The result for an infinite periodic system should be approached by adding a small imaginary part to  $Q$ :  $Q \rightarrow Q + i\epsilon$ , where  $\epsilon \gg \frac{1}{(2N+1)L}$ . Hence the dominant term in  $t(k)$  is given by

$$\sec(Q(2N+1)L) \propto e^{iQ(2N+1)L}$$

and

$$\hat{\tau}(k) \xrightarrow{N \rightarrow \infty} i \frac{dQ}{dE}. \quad (18)$$

For the  $Q$  values defined on the real axis, this conclusion may be justified by considering the averaged tunneling time per unit cell,

$$\langle \hat{\tau}(k) \rangle = \frac{1}{2\epsilon} \int_{k-\epsilon}^{k+\epsilon} \hat{\tau}(p) dp \xrightarrow{N \rightarrow \infty} i \frac{dQ}{dE}. \quad (19)$$

Hence the fast oscillation is smoothed out. Although Eq. (19) is not rigorously proved in this work, it can be checked rather straightforwardly in numerics, and the rigorous mathematical proof may be accomplished by using a stationary phase approximation. The physical meaning of the averaged tunneling time per unit cell may be understood as follows: due to limited resolution, the experimental device is usually only able to measure the averaged result for fast oscillating objects. Figures 1 and 2 show typical examples of plots of  $\hat{\tau}$  for a small-sized system compared with  $i \frac{dQ}{dE}$ . As we can see in Figs. 1 and 2, even for a small-sized system with only just a few cells, the band structures of a totally periodic system already start building up and becoming clearly visible. For finite-size  $\mathcal{PT}$ -symmetric barriers,  $\hat{\tau}_{1,2}$  oscillate around the asymptotic result of  $\langle \hat{\tau}_{1,2} \rangle$  at the large- $N$  limit (note that we use dimensionless quantities in all figures).

The effect of exceptional points (EPs) that separate the broken and unbroken  $\mathcal{PT}$ -symmetric phases in a totally periodic infinite system [58–61] is also visible in a small-sized system; see the dip near  $k \sim 4.1$  in Fig. 2(a). Near the exceptional points,  $\frac{dQ}{dE} \sim 0$ ,  $\langle \hat{\tau}_{1,2} \rangle$  approach zero, and  $\mathcal{PT}$ -symmetric

barriers become almost transparent. This phenomenon is usually referred to as unidirectionally invisibility; see, e.g., Refs. [34,62]. The negative  $\hat{\tau}_1$  near the EP in Fig. 2(a) is distinctive from the positive tunneling time in a real potential scattering theory. In the  $\mathcal{PT}$ -symmetric systems,  $\hat{\tau}_1$  may turn negative due to the fact that the generalized density of states of a  $\mathcal{PT}$ -symmetric system is not positive-definite. The value of  $\tau_1$  turning negative has a strong association with the spectral singularities of the  $\mathcal{PT}$ -symmetric system. When the poles of  $\tau_E$  move across the real axis in the complex  $E$ -plane, they yield drastic and even divergent enhancement near spectral singularities. If the spectral singularities are located within the band, the crossing of poles on the real axis may cause the sign flip of  $\tau_1$ . Following the motion of a pole across the real axis from an unphysical sheet into a physical sheet, the peak of enhancement thus moves toward positive infinity that is connected with negative infinity, and then the sign flips and it continues moving away from negative infinity. A detailed discussion about the effect of spectral singularities is given in Sec. V.

We also remark that the sign of  $Q$  in Eq. (16) is not well-defined and is physically ambiguous. The determination of the sign of  $Q$  must be based on the sign of  $\hat{\tau}_E$ . The ambiguity of multivalued functions in physics is in fact quite common. For example, the ambiguity of the nonanalyticity of the scattering amplitude in some singularity-related cases has been a well-known fact in the analytic  $S$ -matrix approach in nuclear/particle physics; see, e.g., [63,64]. The nature of the nonanalyticity is sometimes not fully determined, and some extra constraint must be imposed on the theory to eliminate the ambiguity, such as, e.g., using the perturbation-theory  $i\epsilon$ -prescription as the reference. As in our case, the ambiguity of the sign of  $Q$  is eliminated by using  $\hat{\tau}_E$  as the reference.

#### V. SPECTRAL SINGULARITIES

With the analytic expressions of the transmission and reflection amplitudes given in Eqs. (14) and (16), it can be easily checked that the traversal time  $\tau_E$  for the  $\mathcal{PT}$ -symmetric model adopted in this work is a well-defined analytic function in the complex  $E$ -plane. Two types of singularities are present: (i) a branch cut sitting along the positive real axis in the complex  $E$ -plane that separate the physical sheet (the first Riemann sheet) and the unphysical sheet (the second Riemann sheet); (ii) poles of the transmission and reflection amplitudes. These poles are called spectral singularities of a non-Hermitian Hamiltonian when they appear on the real axis [65–67], which yields divergences of the reflection and transmission coefficients of the scattered states. The spectral singularities are interpreted as resonance states with vanishing spectral width in Ref. [65].

The motion of the poles in the complex  $E$ -plane has a profound impact on the tunneling of the particle through the  $\mathcal{PT}$ -symmetric barriers. In what follows, we will first discuss the distribution and the properties of pole singularities in Sec. V A. How the value of  $\tau_1$  is affected by the motion of the poles is presented in Sec. V B. The impact of moving poles on some other properties of the tunneling time is discussed in Secs. V C and V A.

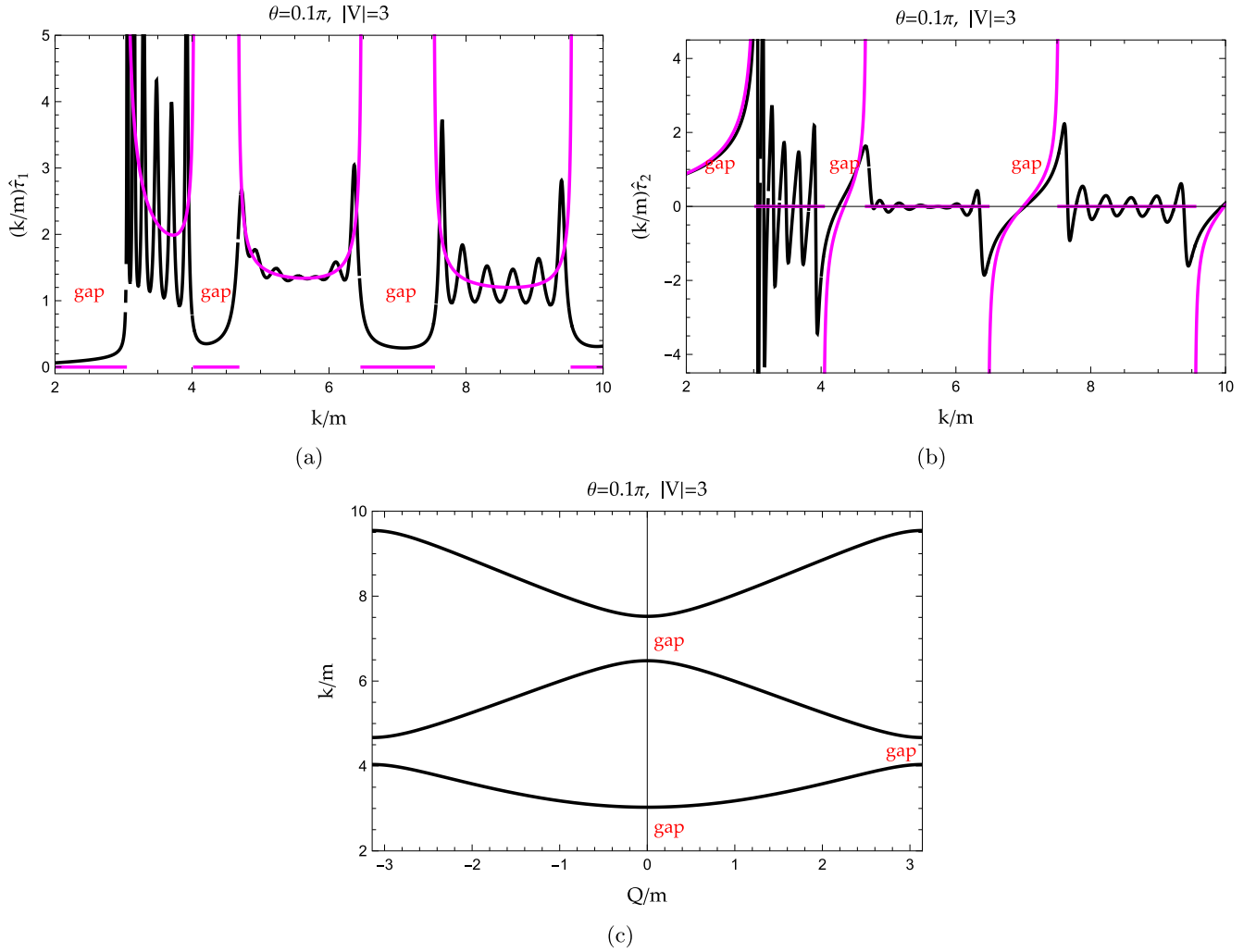


FIG. 1. (a) and (b) Comparison of  $\frac{k}{m}\hat{\tau}$  with  $N = 3$  (solid black) together with  $i\frac{k}{m}\frac{dQ}{dE}$  (solid purple/light gray) vs  $k/m$ . More specifically, (a)  $\frac{k}{m}\hat{\tau}_1$  (solid black) together with  $\frac{k}{m}\frac{d\text{Re}[Q]}{dE}$  (solid purple/light gray); (b)  $\frac{k}{m}\hat{\tau}_2$  (solid black) together with  $\frac{k}{m}\frac{d\text{Im}[Q]}{dE}$  (solid purple/light gray); (c) the corresponding band-structure plot in unbroken  $\mathcal{PT}$ -symmetric phase. The parameters are taken as  $\theta = 0.1\pi$ ,  $|V| = 3$ ,  $mL = 1$ , and  $ma = 0.2$ , where  $|V|$  is dimensionless.

### A. Distribution and motion of poles in a complex plane

The locations of these poles are model-parameter-dependent, and they can be found by solving  $1/t(k) = 0$ . Based on Eq. (14), there are two types of solutions:

(i) Type I singularities are given by solutions of  $\frac{1}{t_0(k)} = 0$ . Hence  $\cos(QL) = 0$  and  $\frac{1}{i(k)} = 0$  are both automatically satisfied, and

$$Q = \frac{\pi}{L} \left( n + \frac{1}{2} \right), \quad n \in \mathbb{Z}. \quad (20)$$

The type I singularities originate from a single cell ( $N = 0$ ), and then they are carried on and shared by the entire many-cell system. The type I solutions hence are independent of the number of cells and the size of the system.

(ii) Type II singularities are system-size-dependent and given by two conditions,

$$\cos(Q(2N+1)L) = 0, \quad \text{Im} \left[ \frac{e^{-ikL}}{t_0(k)} \right] = 0. \quad (21)$$

Using Eqs. (15) and (16), two conditions can be rearranged in the form

$$(x(k), y(k)) = \left( \cos \left( \frac{\pi(n + \frac{1}{2})}{2N+1} \right), \cos \theta \right), \quad (22)$$

where

$$x(k) = \frac{1 - 2 \left[ \frac{m|V|}{k} \sin(k2a) \right]^2}{\cos(kL)},$$

$$y(k) = \frac{1 - 2 \left[ \frac{m|V|}{k} \sin(k2a) \right]^2}{2 \frac{m|V|}{k} \cot(kL)} - \frac{1}{2} \frac{m|V|}{k} \sin(k4a). \quad (23)$$

The  $2N + 1$  independent integer  $n$ 's are labeled as

$$n = 0, 1, \dots, 2N,$$

so  $Q = \frac{\pi(n + \frac{1}{2})}{(2N+1)L}$  sits in the first Brillouin zone. In fact, type I singularity solutions on real axis coincide with solutions of Eq. (22) with  $n = N$ , hence  $Q = \frac{\pi}{2L}$  and  $\cos(QL) = 0$  as

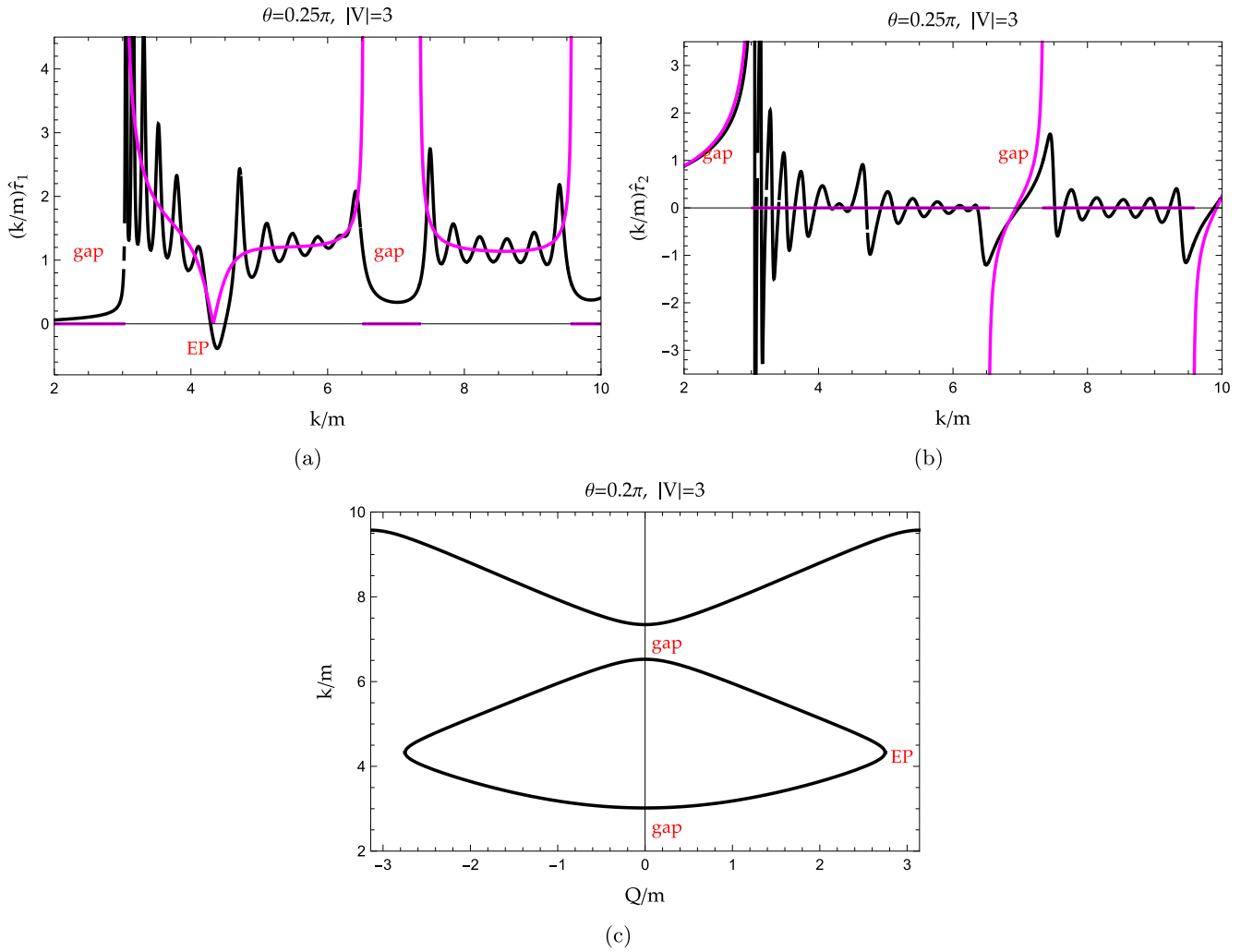


FIG. 2. (a) and (b) Comparison of  $\frac{k}{m}\widehat{\tau}_1$  with  $N = 3$  (solid black) together with  $i\frac{k}{m}\frac{dQ}{dE}$  (solid purple/light gray) vs  $k/m$ . More specifically, (a)  $\frac{k}{m}\widehat{\tau}_1$  (solid black) together with  $\frac{k}{m}\frac{d\text{Re}[Q]}{dE}$  (solid purple/light gray); (b)  $\frac{k}{m}\widehat{\tau}_2$  (solid black) together with  $\frac{k}{m}\frac{d\text{Im}[Q]}{dE}$  (solid purple/light gray); (c) the corresponding band-structure plot in the broken  $\mathcal{PT}$ -symmetric phase. The parameters are taken as  $\theta = 0.2\pi$ ,  $|V| = 3$ ,  $mL = 1$ , and  $ma = 0.2$ , where  $|V|$  is dimensionless.

well for type II solutions with  $n = N$ . However, types I and II solutions of  $n = N$  diverge in a complex plane; see, e.g., Fig. 4.

The solutions of spectral singularities (poles on real axis) can be visualized graphically by plotting parametric curves using both sides of Eq. (22) as  $(x, y)$  coordinates for a fixed  $|V|$ . The intersections of curves indicate the location of spectral singularities; see, e.g., Fig. 3. The distribution of spectral singularity solutions is split up, and poles are clustered into bands with gaps in between (see Fig. 3), where the lowest two bands,  $k/m \in [2.7, 4.52]$  and  $k/m \in [5.24, 6.69]$ , are marked as shadowed areas with red and blue (different gray-scale colors), respectively. As  $N$  is increased, the number of solutions in each band grows linearly. The motion of poles in the complex  $k$ -plane is illustrated in Fig. 4. For  $\theta \sim 0$ , all the poles are located in the unphysical sheet (the second Riemann sheet). As  $\theta$  is increased, some poles start moving across the real axis into the physical sheet (the first Riemann sheet). The critical value of  $\theta_c$  for spectral singularities is individually

dependent; see, e.g., Fig. 4. The density of solutions over a small  $\theta$  interval is controlled by the inverse slope of dashed red (dashed gray) and solid blue (solid gray) curves in Fig. 3; the flatter the curves are, the more spectral singularities are going to cross the real axis over a small range of  $\theta$  increment.

In addition, it is also easy to show, using Eq. (22), that for large  $|V|$  the poles are located around the zeros of  $\sin(2ka)$ . At the limiting case  $|V| \rightarrow \infty$ , poles start approaching  $k = \frac{\pi n}{2a}$ . The physical meaning of such coincidences can be understood by relating them to the formation of resonant states in a single cell, where the distance between two  $\delta$  potentials  $2a$  now plays a dominant role, rather than the length of the cell  $L$ . As a consequence, the electron spends most of its time moving back and forth before leaving the cell. With decreasing  $|V|$ , the poles start moving toward large  $k$ , and the number of poles at the low-energy region decrease and approach zero. Note that in the limit  $kL \ll 1$  and in the first-order Taylor expansion, the positions of the poles do not depend on  $k$ , and the following approximate expression  $m|V_{\text{cr}}| \approx \frac{1}{2a} \sin \frac{\pi}{4} \frac{2n+1}{2N+1}$  can be used to

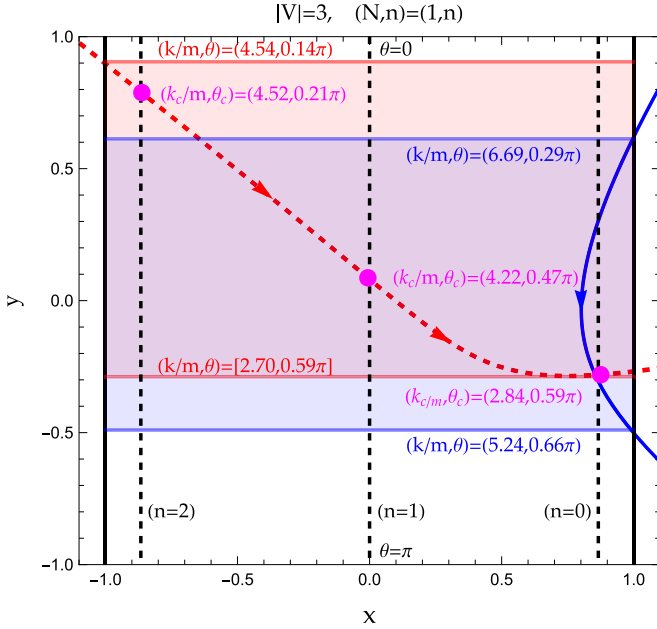


FIG. 3. Spectral singularities condition plot: the parametric plots of the dashed red (dashed gray) and solid blue (solid gray) curves are generated with  $(x, y)$  coordinates given by the left-hand side of Eq. (22) as a function of  $k$ . The dashed black vertical line is generated with coordinates of  $(\cos(\frac{\pi(n+\frac{1}{2})}{2N+1}), \cos\theta)$  with  $N = 1$ ,  $n = 0, 1, 2$ , and  $\theta \in [0, \pi]$ . The arrows indicate increasing  $\theta$  and decreasing  $k$  directions. The value of  $(k, \theta)$  of spectral singularities for fixed  $|V|$  is given by intersection of the dashed black vertical line and the dashed red (dashed gray) and solid blue (solid gray) curves, and marked as purple dots (gray dots). The  $\theta$  values of spectral singularities are indicated by  $\theta'_c$ 's. The shadowed bands represent allowed bands of solutions as  $N \rightarrow \infty$ . The dimensionless parameters are taken as  $|V| = 3$ ,  $mL = 1$ ,  $ma = 0.2$ , and  $N = 1$ .

calculate the critical value  $|V_{cr}|$  for given parameters:  $N$ ,  $n$ , and  $a$ .

### B. Negative $\tau_1$ and its relation to moving poles

In the real potential scattering,  $\tau_1$  always remains positive because of the positivity of the density of states of the systems. However, in  $\mathcal{PT}$ -symmetric systems,  $\tau_1$  is now related to the generalized density of states, which could be either positive or negative and so is  $\tau_1$ . For  $\theta \sim 0$ ,  $\mathcal{PT}$ -symmetric systems behave just like normal real potential systems, and  $\tau_1$  remains positive. As  $\theta$  is increased, the value of  $\tau_1$  may turn negative at certain energy ranges.  $\tau_1$  turning negative is closely related to the motion of poles across the real axis moving from an unphysical sheet (the second Riemann sheet) into a physical sheet (the first Riemann sheet).

For a single cell ( $N = 0$ ), no band structure can be observed yet. The situation is relatively simple. Every time the pole crosses the real axis and moves into the physical sheet, the value of  $\tau_1$  turns negative near the crossing points. An example is illustrated in Fig. 5. For a single cell, only a single spectral singularity can be found near  $k/m = 4.22$  at  $\theta_c = 0.474\pi$ ; see Fig. 4. As we can see in Figs. 5(a)–5(c), for  $\theta < \theta_c = 0.474\pi$ , the pole is still located in the unphysical sheet, and  $\tau_1$ 's values (solid black) are positive. As  $\theta$  ap-

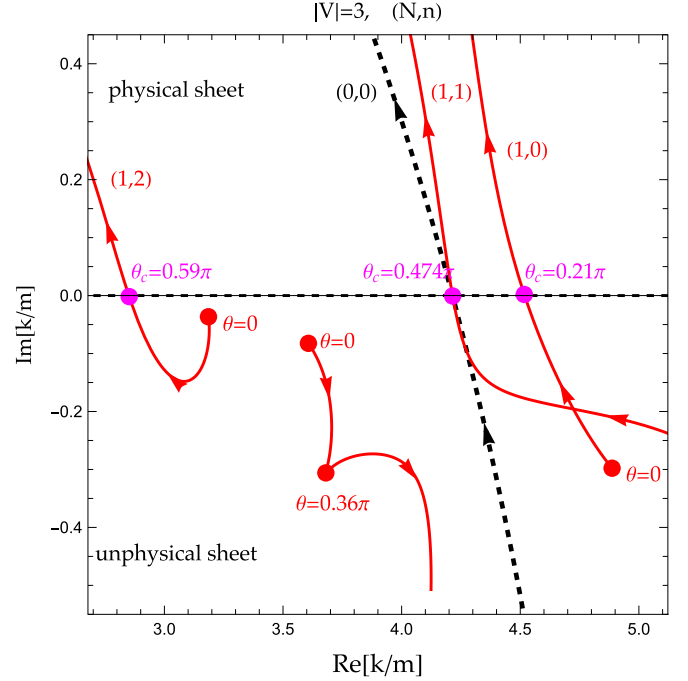


FIG. 4. The motion of poles in the complex  $k/m$ -plane as a function of increasing  $\theta$  for the solutions in the red band in Fig. 3:  $k/m \in [2.7, 4.54]$ ,  $(N, n) = (0, 0)$  (dashed black) and  $(N = 1, n = 0, 1, 2)$  (solid red/solid gray). The arrows indicate increasing  $\theta$  directions. The  $\theta$  values of spectral singularities are indicated by  $\theta'_c$ 's. The dimensionless parameters are taken as  $|V| = 3$ ,  $mL = 1$ ,  $ma = 0.2$ , and  $N = 0, 1$ .

proaches  $\theta_c = 0.474\pi$ , the pole on the unphysical sheet moves towards the real axis, and the peak of enhancement in  $\tau_1$  that is generated by the pole moves up to positive infinity. The spectral singularity at  $\theta = \theta_c$  is a critical point where the peak of positive infinity meets negative infinity. As  $\theta$  is increased and passes over  $\theta_c$  [see Figs. 5(d)–5(f)], the pole now already moves across the real axis into the physical sheet, and the peak in  $\tau_1$  moves across the boundary between positive and negative infinity and turns negative. As  $\theta$  is continuously increased, the pole moves away from the real axis on the physical sheet, which ultimately yields a negative bump near the pole location in  $\tau_1$ . The steepness of the bump is determined by how close the pole is to the real axis. This can be easily demonstrated with the motion of a single pole. Near the pole, the transmission amplitude is approximated by

$$t(k) \propto \frac{1}{k - k_{\text{pole}}} = \frac{k - k_{\text{re}} - i\epsilon}{(k - k_{\text{re}})^2 + \epsilon^2}, \quad (24)$$

where  $k_{\text{pole}} = k_{\text{re}} + i\epsilon$ , with  $k_{\text{re}}$  and  $\epsilon$  being the real and imaginary parts of the pole position. The location of the pole in a physical sheet or an unphysical sheet is determined by the sign of  $\epsilon$ : an unphysical sheet if  $\epsilon < 0$  and a physical sheet if  $\epsilon > 0$ . The  $\tau_1$  near the pole is thus dominated by

$$\tau_1 \sim \frac{m}{k} \frac{\epsilon}{(k - k_{\text{re}})^2 + \epsilon^2}, \quad (25)$$

hence as the pole moves across the real axis into the physical sheet,  $\epsilon$  changes its sign.

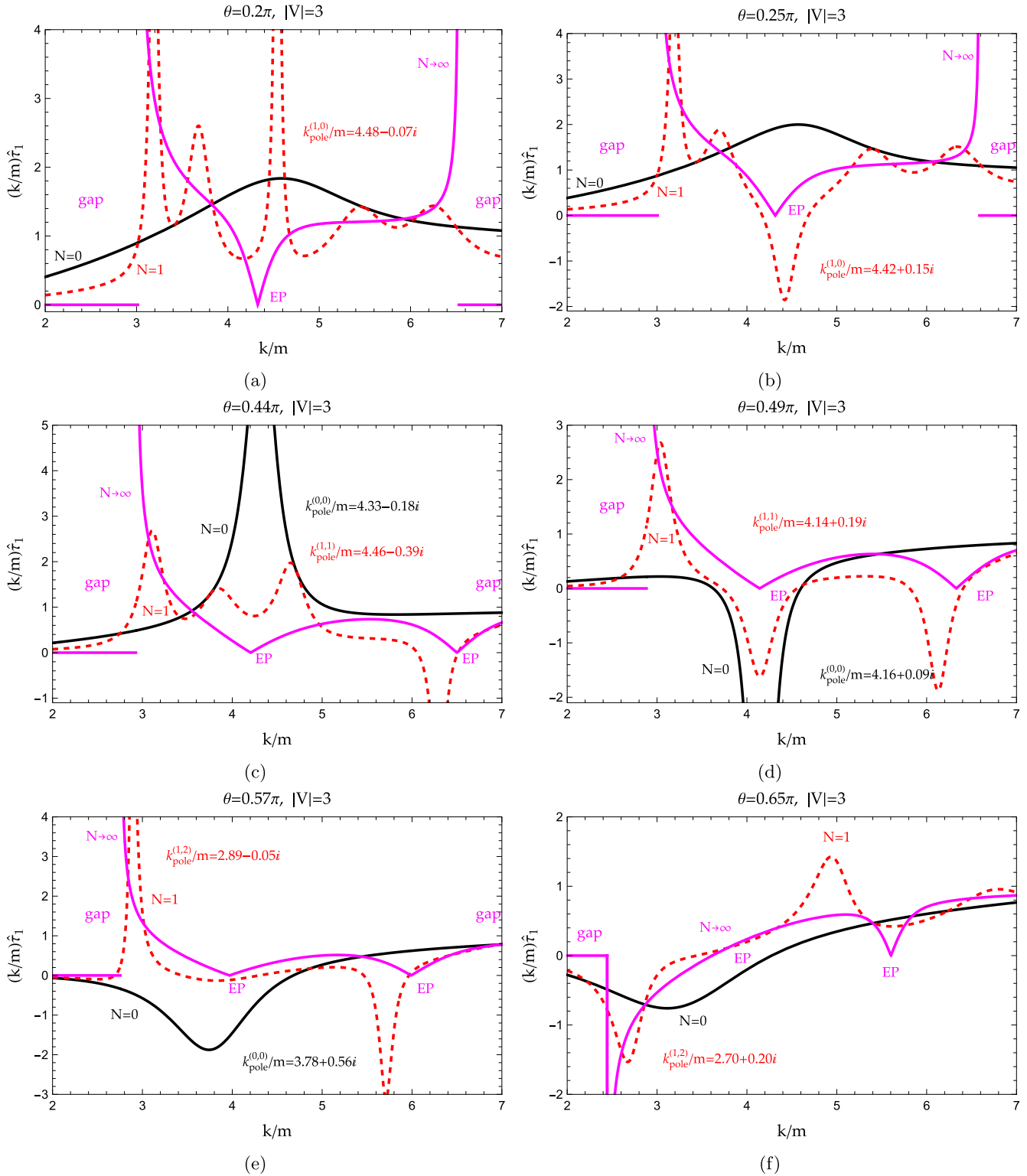


FIG. 5. Plot of  $\frac{k}{m} \hat{\tau}_1$  with  $N = 0$  (solid black),  $N = 1$  (dashed red/dashed gray), together with  $\frac{k}{m} \frac{d \text{Re}[Q]}{dE}$  (solid purple/light gray) vs  $k/m$  for various  $\theta$  values: (a)  $\theta = 0.2\pi$ ; (b)  $\theta = 0.25\pi$ ; (c)  $\theta = 0.44\pi$ ; (d)  $\theta = 0.49\pi$ ; (e)  $\theta = 0.57\pi$ ; (f)  $\theta = 0.65\pi$ . Some of the pole positions near the real axis are listed and marked in red (gray) ( $N = 1$ ) and black ( $N = 0$ ). The dimensionless parameters are taken as  $|V| = 3$ ,  $mL = 1$ , and  $ma = 0.2$ .

In the case of  $N = 1$ , the size of the system is still small, but the band structure already starts appearing. Three spectral singularity solutions can be found within the first cluster of solutions in  $k/m \in [2.7, 4.52]$ ; see Figs. 3 and 4. The locations

are  $k/m = (4.52, 4.22, 2.84)$  at  $\theta_c = (0.21\pi, 0.47\pi, 0.59\pi)$ , respectively. When the first pole crosses the real axis at  $(k/m, \theta_c) = (4.52, 0.21\pi)$  and moves into a physical sheet, it generates a negative bump in  $\tau_1$ ; see Fig. 5(b). As  $\theta$  is



continuously increased near  $\theta_c = 0.47\pi$ , the second pole is getting close to the real axis at  $k/m = 4.22$  and starts competing with the nearby first pole in the physical sheet. It becomes dominant near  $\theta_c = 0.47\pi$ , and it turns  $\tau_1$  back into positive; see Fig. 5(c). After the second pole crosses the real axis, it flips  $\tau_1$  again and generates a negative bump at  $k/m \sim 4.14$ ; see Fig. 5(d). Just as  $\theta$  is continuously increased up to  $\theta_c = 0.59\pi$ , the last pole moves in and becomes the dominant effect in turning  $\tau_1$  when it crosses the real axis near  $k/m \sim 2.7$ ; see Figs. 5(e) and 5(f).

For a large- $N$  system, the situation is even more interesting. The band structure and EPs start getting involved, competing with poles and playing a role in turning  $\tau_1$ . The spectral singularities are clustered into bands; the first band appears in  $k/m \in [2.7, 4.52]$  at corresponding  $\theta \in [0.59\pi, 0.21\pi]$ . For  $\theta \in [0.21\pi, 0.5\pi]$ , spectral singularities and poles are clustered in  $k/m \in [4, 4.5]$ , which happens near the edge of two merging bands (EPs). The effect of poles located near the edge of two merging bands is hence highly suppressed by EPs, and the  $\tau_1$  remain positive. For  $\theta \in [0.5\pi, 0.59\pi]$ , the cluster of spectral singularities and poles now moves up to the lower edge of the band  $k/m \sim 2.8$ , and they become the dominant force in determining the fate of  $\tau_1$ . When they move across the real axis, the  $\tau_1$  in the lower band below EP is turned completely; see the purple (light gray) curves in Figs. 5(e) and 5(f).

Now the physical interpretation of the negative value of  $\tau_1$  as repelling time that is physically inaccessible can be understood in terms of the motion of poles. As we can see in Fig. 5, the turning to negative of  $\tau_1$  is closely related to the motion of the pole crossing the real axis. As the pole crosses the real axis from the unphysical sheet into the physical sheet, the value of  $\tau_1$  experiences the transition process from a positive value to positive infinity that is connected with negative infinity, and ultimately to a negative value.  $\tau_1$  diverges at spectral singularity and generates an infinite sharp barrier for the particle to pass through. As the pole moves into the physical sheet, the barrier is broadened and turned into a negative value band that repels particles. The behavior of  $\tau_2$  is plotted in Fig. 6.

### C. Dispersion integral relation of $\tau_E$

In addition to turning the value of  $\tau_1$ , the motion of pole singularities also has a big impact on the dispersion integral relation of  $\tau_E$ . For the small  $\theta \sim 0$ , all the spectral singularities are located in the unphysical sheet or equivalently in the lower half complex  $k$ -plane with  $\text{Im}[k] < 0$ . Hence, except for the branch cut, no other singularities can be found in the physical sheet, and the  $\tau_E$  must satisfy Cauchy's integral theorem (also referred to as the dispersion integral relation in nuclear/particle physics),

$$\tau_E = \frac{1}{\pi} \int_0^\infty d\omega \frac{\text{Disc}_\omega \tau_\omega}{\omega - E}, \quad (26)$$

where for the  $\mathcal{PT}$ -symmetric system the discontinuity of  $\tau_E$  crossing the branch cut is

$$\text{Disc}_E \tau_E = \text{Im}[\tau_E] = \tau_1(E)$$

for real values of  $E$ . Specifically for the model used in this work, asymptotically  $\tau_1(E) \rightarrow 0$  as either  $E \rightarrow 0$  or  $E \rightarrow \infty$ , hence Cauchy's integral on the right-hand side of Eq. (26) is well-behaved and converging. No subtractions or extra constant terms are needed.

As  $\theta$  is continuously increased, poles of transmission and reflection amplitudes start moving around in a complex plane. Some move across the branch cut on the real axis and start to interfere with a Cauchy integration contour; see, e.g., Fig. 4. When poles from the unphysical sheet move across the branch cut into the physical sheet, the contour of the Cauchy integral is dragged to follow the motion of the poles and move together with them. The residue contribution of the poles in the physical sheet thus must be picked up due to the deformation of the contour of the Cauchy integral, hence Eq. (26) is modified to

$$\tau_E = \sum_i \left[ \frac{2i \text{Res}_{\text{pole}-i}}{E - E_{\text{pole}-i}} - \frac{2i \text{Res}_{\text{pole}-i}^*}{E - E_{\text{pole}-i}^*} \right] + \frac{1}{\pi} \int_0^\infty d\omega \frac{\text{Disc}_\omega \tau_\omega}{\omega - E}, \quad (27)$$

where  $E_{\text{pole}-i}$  stands for the position of the  $i$ th pole. The residue of the  $i$ th pole of the  $\text{Disc}_E \tau_E$  function,  $\text{Res}_{\text{pole}-i}$ , is given by

$$\text{Res}_{\text{pole}-i} = (E - E_{\text{pole}-i}) \text{Disc}_E \tau_E |_{E \rightarrow E_{\text{pole}-i}}. \quad (28)$$

For complex  $E$ , the  $\text{Disc}_E \tau_E$  function must be generalized to

$$\text{Disc}_E \tau_E = \frac{\tau_E - \tau_{E^*}}{2i}. \quad (29)$$

The poles of transmission and reflection amplitudes in  $\mathcal{PT}$ -symmetric systems always show up in complex-conjugate pairs. In terms of momenta, the conjugate pair,  $E_{\text{pole}-i}$  and  $E_{\text{pole}-i}^*$ , is associated with  $k_{\text{pole}-i}$  and  $-k_{\text{pole}-i}^*$ , respectively. The pair of conjugate pole terms together guarantees that all the pole terms in Eq. (27) are always real for  $E$  on the real axis. Equation (27) can be checked numerically rather straightforwardly for a small- $N$  system; see, e.g., Fig. 7. As  $N$  grows, the number of poles soon becomes too large to manage.

## VI. DISCUSSION AND SUMMARY

### A. Large- $N$ limit in the presence of spectral singularities?

The averaging tunneling time in Eq. (18) works well and is mathematically well-defined in bands where spectral singularities are absent on a real axis, and the poles are all either in a physical sheet or they have already crossed the real axis into an unphysical sheet. However, in the bands where the divergent singularities show up on the real axis and the band is still in the middle of a transition between the all positive and the all negative band of  $\tau_1$  (see, e.g., Fig. 8), Eq. (18) breaks down, and the large- $N$  limit becomes ambiguous and problematic. Now we are facing the following question: is there a physically meaningful large- $N$  limit in the region where divergent singularities show up? Should we even bother to ask such a question? Or perhaps is the size-dependent fast oscillating and divergent behavior in the  $\tau_1$  region the nature of  $\mathcal{PT}$ -symmetric systems? If such a limit indeed exists, should the size-dependent type II spectral singularities be all smoothed and washed out? Is a large-size periodic system supposed to be free of type II spectral singularities? We still do not have a clear answer to these questions.

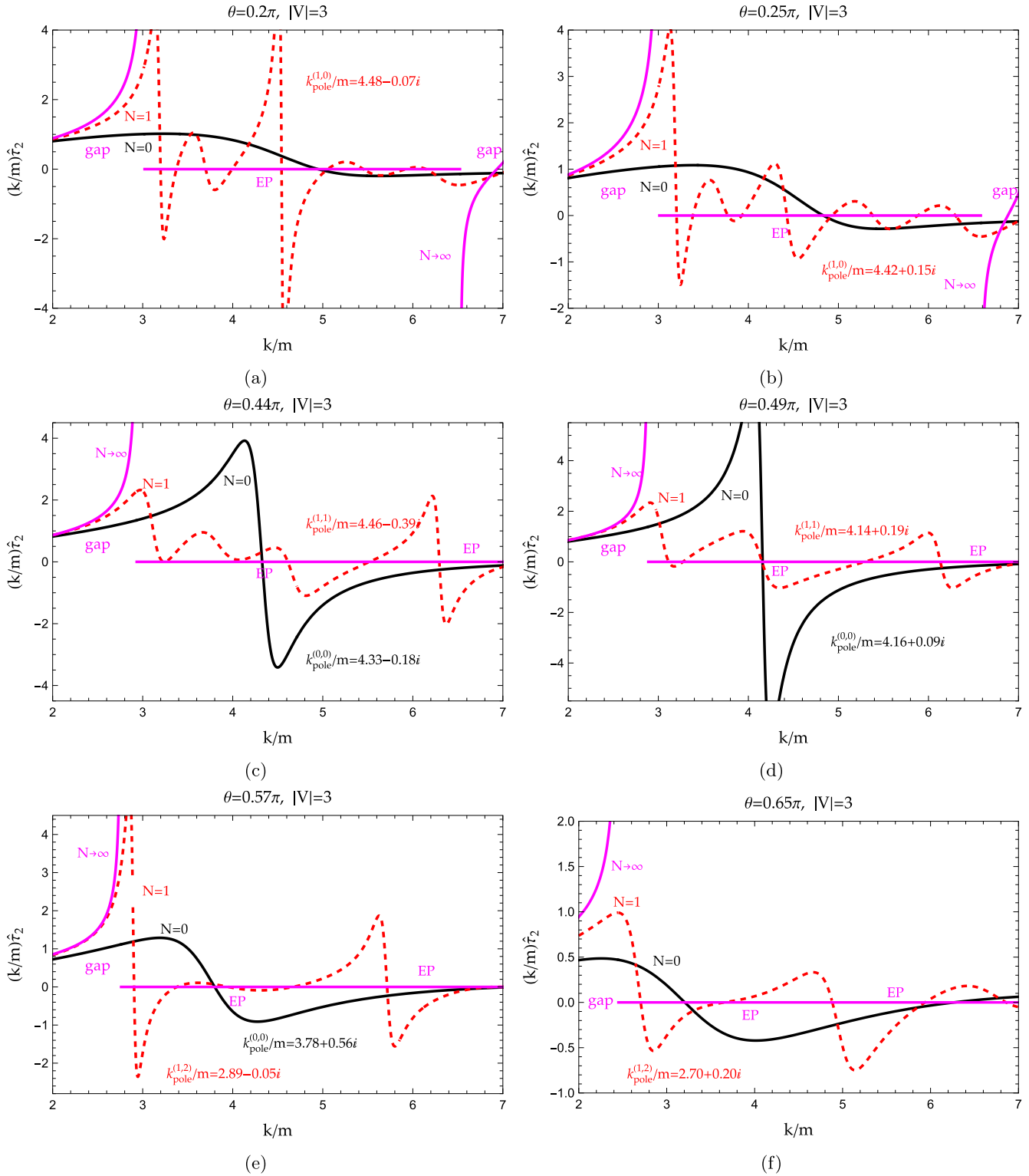


FIG. 6. Plot of  $\frac{k}{m} \hat{\tau}_2$  with  $N = 0$  (solid black),  $N = 1$  (dashed red/dashed gray), together with  $\frac{k}{m} \frac{d \text{Im}[Q]}{dE}$  (solid purple/light gray) vs  $k/m$ , for various  $\theta$  values: (a)  $\theta = 0.2\pi$ ; (b)  $\theta = 0.25\pi$ ; (c)  $\theta = 0.44\pi$ ; (d)  $\theta = 0.49\pi$ ; (e)  $\theta = 0.57\pi$ ; (f)  $\theta = 0.65\pi$ . Some of the pole positions near the real axis are listed and marked in red (gray) ( $N = 1$ ) and black ( $N = 0$ ). The dimensionless parameters are taken as  $|V| = 3$ ,  $mL = 1$ , and  $ma = 0.2$ .

One very interesting observation is that as  $N \rightarrow \infty$ , solutions of poles are pushed either towards or far away from the real axis. This can be understood because the pole position depends on factors such as  $e^{iQ(2N+1)L}$  and  $e^{ik(2N+1)L}$ , hence as

$N \rightarrow \infty$ , two factors either grow fast or decay exponentially for  $Q$  and  $k$  in a complex plane. The divergence of spectral singularities may be removed by computing the value of  $\hat{\tau}(k \pm i\epsilon)$  away from singularities where  $\epsilon$  is much larger than

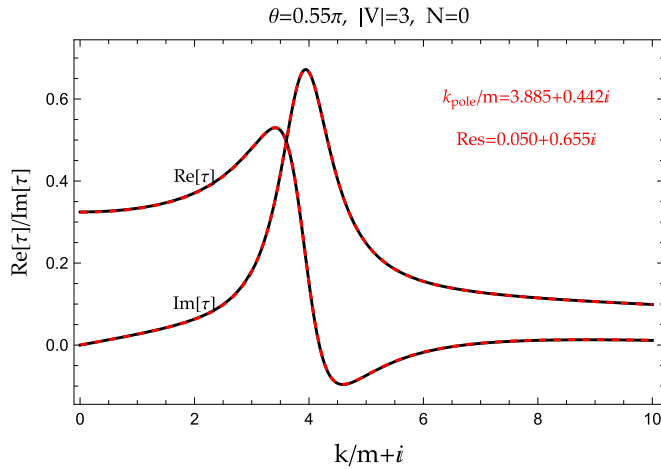


FIG. 7. The plot of the real and imaginary parts of  $\tau_E$  by the dispersion integral relation in Eq. (27) (solid black) together with  $\tau_E$  (dashed red/gray) for  $N = 0$  (the curves overlap). Only one pole is present at  $k/m = 3.885 + 0.442i$ .  $\tau_E$  is computed and shown off the real  $E$  axis only for the purpose of fast convergence of the Cauchy integral. The parameters are taken as  $\theta = 0.55\pi$ ,  $|V| = 3$ ,  $mL = 1$ , and  $ma = 0.2$ , where  $|V|$  is dimensionless.

the imaginary part of the pole solutions. However, similar to the ambiguity in the sign of  $Q$ , for the band that is still in the middle of the transition, some parts of it have already turned negative but other parts remain positive, and now we are facing the ambiguity of shifting  $k$  above or below singularities. In addition, one may also wonder how energy can be accessed in a complex plane. The idea proposed by Lloyd in Ref. [68] may shed some light on this question: the averaged Green's function of a disordered system with Cauchy-type uncorrelated disorder is equal to the Green's function of an ordered system with the energy argument shifted into a complex plane.

### B. Summary

In summary, the concept of tunneling time is generalized and applied to  $\mathcal{PT}$ -symmetric systems. The distinctive features and properties of the tunneling time in  $\mathcal{PT}$ -symmetric systems are studied and discussed by using a simple exactly solvable diatomic  $\mathcal{PT}$ -symmetric impurities model. Unlike the positive-definite  $\tau_1$  in real potential scattering theory, the  $\tau_1$  in  $\mathcal{PT}$ -symmetric systems can be either positively or negatively valued. The value of  $\tau_1$  turning negative is closely related to the motion of pole singularities of scattering amplitudes in a complex  $k$ -plane. When the poles are all located in an unphysical sheet (the second Riemann sheet),  $\tau_1$  remains positive. As poles move close to and ultimately cross the real axis into a physical sheet (the first Riemann sheet), the poles generate an enhancement in  $\tau_1$  near the location of the poles. The peak of enhancement moves into positive infinity and then back in from negative infinity with the sign flipped. For large-sized systems, the situation is even more intriguing. The band structure of the system is clearly visible for even small-sized systems. The number of poles grows drastically with size, and the distribution of poles splits into bands. When the poles show up inside an allowed band of a system and all move across the real axis, they tend to flip

the sign of the entire band. In some bands where two bands start merging together at an exceptional point (EP), the EPs tend to force  $\tau_1$  to approach zero and start to compete with the poles, so  $\mathcal{PT}$ -symmetric systems become almost transparent near the EPs. The fate of  $\tau_1$  near EPs is now the result of two competing forces: the poles and the EPs.

The negative value of  $\tau_1$  is a distinctive feature of  $\mathcal{PT}$ -symmetric systems as a consequence of norm violation, hence it may be used to quantify and calibrate the degree of norm violation in  $\mathcal{PT}$ -symmetric systems even with balanced gain and loss. In addition, the negative value portion of  $\tau_1$  is physically inaccessible and behaves just like a forbidden gap in conventional periodic real potential systems. Therefore, by manipulating balanced gain and loss in a  $\mathcal{PT}$ -symmetric system, we may be able to manufacture a new type of band-structure electronic or optical devices even for a small finite-size nonperiodic system.

The impact of spectral singularities on the dispersion integral relation of  $\tau_E$  and the large- $N$  limit is also discussed. As poles move across the real axis into a physical sheet, the contour of the Cauchy integral must be deformed and follow the motion of the poles, hence the residue terms must be picked up in a dispersion integral relation of  $\tau_E$ . In the band of absent spectral singularities, the large- $N$  limit is well defined and can be achieved by either averaging the fast oscillating behavior of  $\tau_E$  or using  $i\epsilon$ -prescription by shifting  $k$  off the real axis into a complex plane. However, in the bands that are plagued by divergent spectral singularities, defining a large- $N$  limit becomes problematic. The question of how to define a physically meaningful large- $N$  limit in the presence of spectral singularities is still open.

### ACKNOWLEDGMENTS

P.G. and V.G. acknowledge support from the Department of Physics and Engineering, California State University, Bakersfield, CA. V.G. and E.J. would like to thank UPCT for partial financial support through the concession of "Maria Zambrano ayudas para la recualificaci3n del sistema universitario espa3ol 2021-2023" financed by Spanish Ministry of Universities with financial funds "Next Generation" of the EU.

### APPENDIX A: PARTICLE SCATTERING BY AN ARRAY OF PERIODIC $\mathcal{PT}$ -SYMMETRIC CELLS

Considering the scattering of a spinless particle of mass  $m$  by assembly of periodic  $\mathcal{PT}$ -symmetric cells, the dynamics is described by the one-dimensional Schr3dinger equation along the incident direction  $x$ ,

$$\left[ -\frac{1}{2m} \frac{d^2}{dx^2} + \sum_{n=-N}^N V(x-nL) \right] \Psi_E(x) = E \Psi_E(x), \quad (\text{A1})$$

where  $V(x)$  stands for the potential in a unit cell.  $2N + 1$  cells are placed symmetrically on both sides of the origin. The length of scattering barriers is thus  $(2N + 1)L$ , where  $L$  denotes the length of a single cell. Inside of each single cell, we adopt a simple  $\mathcal{PT}$ -symmetric impurities model with a

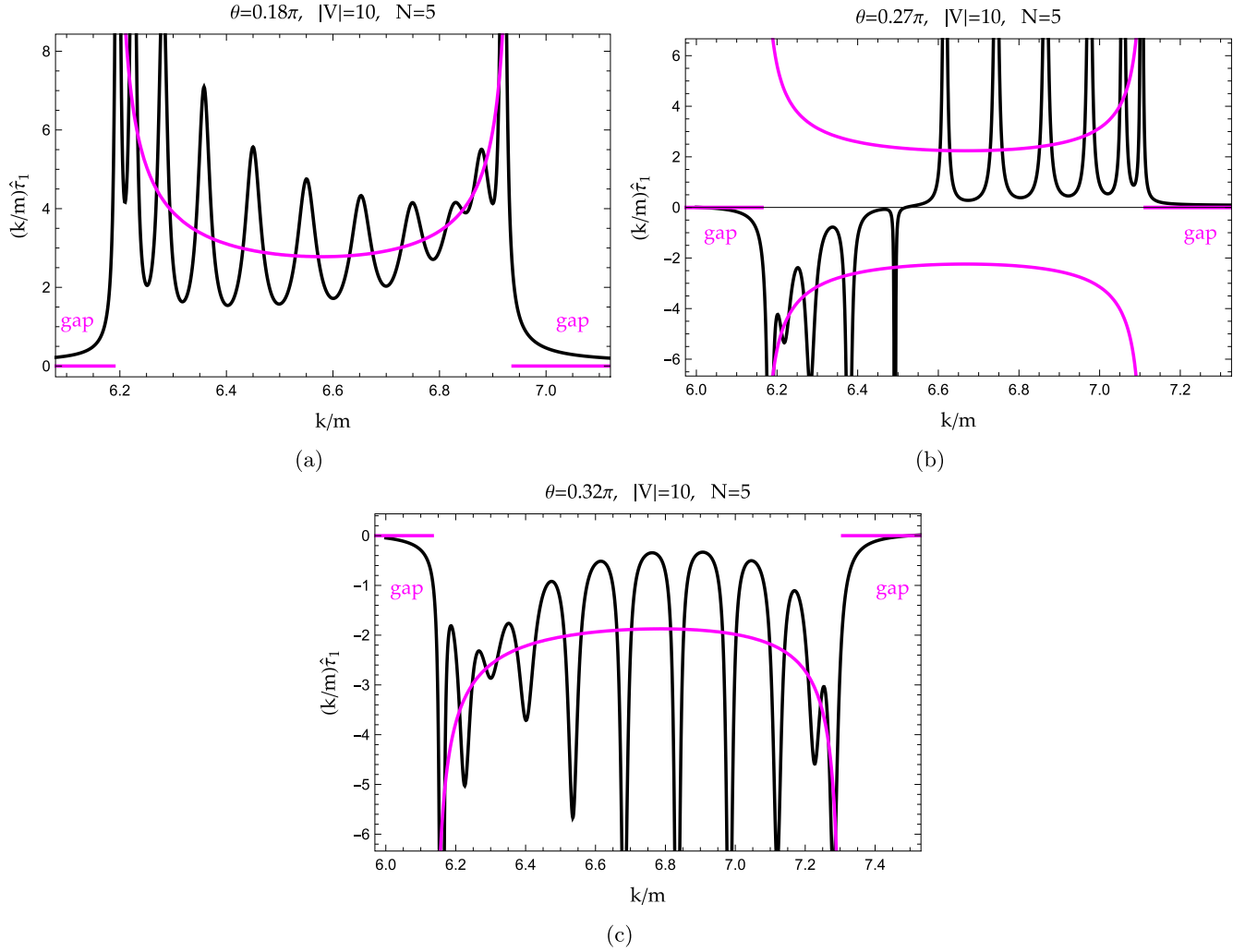


FIG. 8. Plot of  $\frac{k}{m} \widehat{\tau}_1$  with  $N = 5$  and  $|V| = 10$  (solid black) together with  $\frac{k}{m} \frac{d \operatorname{Re}[Q]}{dE}$  (solid purple/light gray) for various  $\theta$  values: (a)  $\theta = 0.18\pi$ ; (b)  $\theta = 0.27\pi$ ; (c)  $\theta = 0.32\pi$ . The rest of the parameters are taken as  $mL = 1$  and  $ma = 0.2$ .

potential,

$$V(x) = V\delta(x - a) + V^*\delta(x + a), \quad V = |V|e^{i\theta}. \quad (\text{A2})$$

Two contact interactions with complex strength that are conjugate to each other are placed on two sides of the cell's center at an equal distance  $a$ , thus the potential satisfies the  $\mathcal{PT}$  symmetry relation,

$$V(-x) = V^*(x). \quad (\text{A3})$$

For scattering solutions, it is more convenient to consider the Lippmann-Schwinger (LS) equation,

$$\begin{aligned} \Psi_E(x) &= \Psi_E^{(0)}(x) + \sum_{n=-N}^N \int_{-\infty}^{\infty} dx' G_0(x - x'; E) \\ &\quad \times V(x' - nL) \Psi_E(x'), \end{aligned} \quad (\text{A4})$$

where

$$\Psi_E^{(0)}(x) = Ae^{ikx} + Be^{-ikx} \quad (\text{A5})$$

represents the incident waves with linear superposition of both left- and right-propagating plane waves, and

$$k = \sqrt{2m(E + i0)}$$

stands for the linear momentum of an incident particle. The Green's function of a free particle,  $G_0(x; E)$ , is given by

$$G_0(x; E) = \int_{-\infty}^{\infty} \frac{dp}{2\pi} \frac{e^{ipx}}{E - \frac{p^2}{2m}} = -\frac{im}{k} e^{ik|x|}. \quad (\text{A6})$$

With the contact interaction potential given in Eq. (A2), the scattering dynamics is thus totally determined by discrete LS equations on scattering sites,

$$\sum_{n'=-N}^N [D(k)]_{n,n'} \begin{bmatrix} \Psi_E(n'L + a) \\ \Psi_E(n'L - a) \end{bmatrix} = \begin{bmatrix} \Psi_E^{(0)}(nL + a) \\ \Psi_E^{(0)}(nL - a) \end{bmatrix}, \quad (\text{A7})$$

where

$$[D(k)]_{n,n'} = \begin{bmatrix} \delta_{n,n'} + \frac{imV}{k} e^{ik|n-n'|L} & \frac{imV^*}{k} e^{ik|nL-n'L+2a|} \\ \frac{imV}{k} e^{ik|nL-n'L-2a|} & \delta_{n,n'} + \frac{imV^*}{k} e^{ik|n-n'|L} \end{bmatrix}. \quad (\text{A8})$$

The on-energy-shell scattering amplitudes can be easily pulled out by considering the asymptotic form of the wave function,

$$\Psi_E(x) \stackrel{|x| \gg NL}{\approx} \Psi_E^{(0)}(x) + i f_E(p) e^{ik|x|}, \quad p = \frac{x}{|x|} k, \quad (\text{A9})$$

where

$$f_E(p) = - \sum_{n=-N}^N e^{-ipnL} \left[ \frac{mV}{k} e^{-ipa} \Psi_E(nL+a) + \frac{mV^*}{k} e^{ipa} \Psi_E(nL-a) \right]. \quad (\text{A10})$$

Using Eq. (A7), the formal solution of the scattering amplitude with a general incident wave,  $Ae^{ikx} + Be^{-ikx}$ , is thus given by

$$f_E(p) = - \sum_{n,n'=-N}^N e^{-ipnL} \left[ \frac{mV}{k} e^{-ipa} \quad \frac{mV^*}{k} e^{ipa} \right] [D^{-1}(k)]_{n,n'} \times \begin{bmatrix} \Psi_E^{(0)}(n'L+a) \\ \Psi_E^{(0)}(n'L-a) \end{bmatrix}. \quad (\text{A11})$$

The  $S$ -matrix in a left/right-propagating wave basis—(R)  $A = 1$  and  $B = 0$ ; (L)  $A = 0$  and  $B = 1$ —is defined by

$$S(E) = \begin{bmatrix} t(k) & r^{(L)}(k) \\ r^{(R)}(k) & t(k) \end{bmatrix}, \quad (\text{A12})$$

where  $t(k)$  and  $r^{(L/R)}(k)$  are transmission and left/right reflection amplitudes, and they are related to the left/right basis scattering amplitudes by

$$t(k) = 1 + i f_E^{(R)}(k) = 1 + i f_E^{(L)}(-k), \\ r^{(R)}(k) = i f_E^{(R)}(-k), \quad r^{(L)}(k) = i f_E^{(L)}(k). \quad (\text{A13})$$

Transmission and reflection amplitudes can be parametrized by three real functions: one inelasticity  $\eta(k) \in [1, \infty]$  and two phase shifts  $\delta_{\pm}(k)$  (see Ref. [40]),

$$t = \eta \cos(\delta_+ - \delta_-) e^{i(\delta_+ + \delta_-)}, \\ r^{(R/L)} = i[\eta \sin(\delta_+ - \delta_-) \pm \sqrt{\eta^2 - 1}] e^{i(\delta_+ + \delta_-)}. \quad (\text{A14})$$

The inelasticity and phase shifts are linked to scattering amplitudes directly by the relations (see Ref. [40]),

$$\frac{\eta(k) e^{2i\delta_{\pm}(k)} - 1}{2i} = \frac{[f^{(R)}(k) \pm f^{(L)}(k)] \pm [f^{(R)}(-k) \pm f^{(L)}(-k)]}{4}. \quad (\text{A15})$$

For a  $\mathcal{PT}$ -symmetric system, using relations given in Eq. (A14), one can easily verify that

$$\frac{1}{2i} \ln \det [S(E)] = \delta_+(k) + \delta_-(k) = \text{Im}[\ln t(k)]. \quad (\text{A16})$$

In addition, another very useful relation between transmission amplitude and the  $D(k) = 1 - G_0(k)V$  matrix defined in Eq. (A8) is given by

$$t(k) = \frac{1}{\det [D(k)]}. \quad (\text{A17})$$

This relation can be proven by using the properties of the  $S$ -matrix. The  $S$ -matrix operator is related to the  $D$ -matrix operator by [see Eqs. (12), (24), and (27) in Ref. [40]]

$$\hat{S}(E) = \frac{\hat{D}(-k)}{\hat{D}(k)}, \quad \pm k = \sqrt{2m(E \pm i0)}, \quad (\text{A18})$$

where  $\hat{D}(\pm k)$  are defined below and above branch cut singularity of the analytic  $\hat{D}$ -matrix operator, respectively, and the branch cut is sitting on the real energy axis. Hence we obtain

$$\frac{1}{2i} \ln \det [S(E)] = -\text{Im}[\ln \det [D(k)]] = \text{Im}[\ln t(k)]. \quad (\text{A19})$$

Both  $t(k)$  and  $\det [D(k)]$  are analytic functions defined in the entire complex  $E$ -plane. The real parts of the two functions are related to the imaginary parts by the Cauchy integral, which ultimately yields the relation (A17).

### 1. Analytic scattering solutions by the LS equation approach

For the simple contact interaction  $\mathcal{PT}$ -symmetric model, it turns out that the scattering solutions can be obtained analytically. The discrete LS equations in Eq. (A7) can be solved by assuming

$$\begin{bmatrix} \Psi_E(nL+a) \\ \Psi_E(nL-a) \end{bmatrix} = \begin{bmatrix} C & D \\ E & F \end{bmatrix} \begin{bmatrix} \cos(QnL) \\ i \sin(QnL) \end{bmatrix}. \quad (\text{A20})$$

That is, the wave functions at the scattering sites are determined completely by collective modes of the entire lattice of impurities, and hence they are described by plane waves with a wave vector  $Q$ . All the coefficients ( $C, D, E, F$ ) and the wave vector  $Q$  can be determined by plugging Eq. (A20) into Eq. (A7). Using the identities

$$\sum_{n'=-N}^N e^{ik|nL-n'L+d|} \cos(Qn'L) \\ = i \frac{\sin(k|d| - kL) - \sin(k|d|) \cos(QL)}{\cos(kL) - \cos(QL)} \cos(QnL) \\ + i \frac{\sin(kd) \sin(QL)}{\cos(kL) - \cos(QL)} \sin(QnL) \\ - C(k) \cos(knL + kd) \quad (\text{A21})$$

and

$$\sum_{n'=-N}^N e^{ik|nL-n'L+d|} \sin(Qn'L) \\ = i \frac{\sin(k|d| - kL) - \sin(k|d|) \cos(QL)}{\cos(kL) - \cos(QL)} \sin(QnL) \\ - i \frac{\sin(kd) \sin(QL)}{\cos(kL) - \cos(QL)} \cos(QnL) \\ + i S(k) \sin(knL + kd), \quad (\text{A22})$$

where  $d = \pm 2a$ , and

$$C(k) = \frac{[\cos(Q(N+1)L) - \cos(QNL)] e^{ikL}}{\cos(kL) - \cos(QL)}, \\ S(k) = \frac{[\sin(Q(N+1)L) - \sin(QNL)] e^{ikL}}{\cos(kL) - \cos(QL)}, \quad (\text{A23})$$

comparing both sides of Eq. (A7), all the coefficients of the independent plane waves,  $(\cos(QnL), \sin(QnL))$  and  $(\cos(knL), \sin(knL))$ , must all vanish. Hence, we find

$$Q = \frac{1}{L} \arccos \left[ \cos(kL) + \frac{m|V|}{k} 2 \cos \theta \sin(kL) + 2 \left( \frac{m|V|}{k} \right)^2 \sin(k2a) \sin(kL - k2a) \right]. \quad (\text{A24})$$

The relation given in Eq. (A24) is in fact the exact energy-momentum dispersion relation when  $N \rightarrow \infty$  and the

$\mathcal{PT}$ -symmetric system or a diatomic crystal system becomes totally periodic; see, e.g., Refs. [48,69]. The wave vector  $Q$  hence plays the role of crystal momentum, where a crystal is formed by all the impurities placed at the interaction sites. We also remark that even though for a finite system the wave function at interaction sites is indeed periodic and simply given by Bloch waves,  $\Psi_E(nL \pm a) \propto e^{\pm iQnL}$ , the entire wave function is not periodic and does not satisfy the Bloch theorem.

The coefficients  $C$  and  $D$  are given by the solutions of the coupled algebra equations,

$$\begin{aligned} \cos(ka)\mathbb{C}(k) \left[ \left( 1 + \frac{mV^*}{k} \alpha \right) C + \frac{mV^*}{k} \beta D \right] + \sin(ka)\mathbb{S}(k) \left[ \left( 1 - \frac{mV^*}{k} \alpha \right) D - \frac{mV^*}{k} \beta C \right] &= -\frac{A+B}{\frac{imV}{k}}, \\ \sin(ka)\mathbb{C}(k) \left[ \left( 1 - \frac{mV^*}{k} \alpha \right) C - \frac{mV^*}{k} \beta D \right] + \cos(ka)\mathbb{S}(k) \left[ \left( 1 + \frac{mV^*}{k} \alpha \right) D + \frac{mV^*}{k} \beta C \right] &= -\frac{A-B}{\frac{imV}{k}}, \end{aligned} \quad (\text{A25})$$

where

$$\alpha = \frac{\sin(k2a - kL) - \sin(k2a) \cos(QL)}{\cos(kL) - \cos(QL) + \frac{mV^*}{k} \sin(kL)}, \quad \beta = \frac{i \sin(k2a) \sin(QL)}{\cos(kL) - \cos(QL) + \frac{mV^*}{k} \sin(kL)}. \quad (\text{A26})$$

The coefficients  $E$  and  $F$  are related to  $C$  and  $D$  by

$$E = \frac{mV}{k} (\alpha C + \beta D), \quad F = \frac{mV}{k} (\beta C + \alpha D). \quad (\text{A27})$$

Using Eqs. (A20) and (A10), the analytic expression of the scattering amplitude is given by

$$f_E(p) = -\frac{mV}{k} \left[ \frac{mV^*}{k} e^{ipa} [\alpha \Omega_c(p) + \beta \Omega_s(p)] + e^{-ipa} \Omega_c(p) \right] C - \frac{mV}{k} \left[ \frac{mV^*}{k} e^{ipa} [\beta \Omega_c(p) + \alpha \Omega_s(p)] + e^{-ipa} \Omega_s(p) \right] D, \quad (\text{A28})$$

where

$$\begin{aligned} \Omega_c(p) &= \sum_{n=-N}^N e^{-ipnL} \cos(QnL) = \frac{\cos(k(N+1)L) \cos(QNL) - \cos(kNL) \cos(Q(N+1)L)}{\cos(pL) - \cos QL}, \\ \Omega_s(p) &= \sum_{n=-N}^N e^{-ipnL} i \sin(QnL) = \frac{\sin(k(N+1)L) \sin(QNL) - \sin(kNL) \sin(Q(N+1)L)}{\cos(pL) - \cos QL}. \end{aligned} \quad (\text{A29})$$

After some lengthy and highly nontrivial calculation, compact forms of the transmission and reflection amplitudes can be found,

$$\begin{aligned} [t(k) e^{ik(2N+1)L}]^{-1} &= \det[D(k)] e^{-ik(2N+1)L} \\ &= \cos(Q(2N+1)L) - i \sin(kL) \frac{\sin(Q(2N+1)L)}{\sin(QL)} + 2 \frac{im|V|}{k} \cos \theta \cos(kL) \frac{\sin(Q(2N+1)L)}{\sin(QL)} \\ &\quad + 2i \left( \frac{m|V|}{k} \right)^2 \sin(k2a) \cos(kL - k2a) \frac{\sin(Q(2N+1)L)}{\sin(QL)}, \end{aligned} \quad (\text{A30})$$

and

$$r^{(R/L)}(k) = -\frac{\frac{im|V|}{k} \sin(Q(2N+1)L)}{\det[D(k)] \sin(QL)} 2 \left[ \cos(k2a \pm \theta) + \frac{m|V|}{k} \sin(k2a) \right]. \quad (\text{A31})$$

## 2. Characteristic determinant approach

The analytic solutions can also be obtained elegantly by the characteristic determinant approach that was developed in Refs. [47–49]. The key idea is to take advantage of recursion relations that the determinant of the  $D$ -matrix in Eq. (A8) must satisfy. Starting with a single impurity, by adding one impurity at a time and using recursion relations, the expression of the determinant of the  $D$ -matrix of a finite-size multiple cells system can be obtained.

The general idea of the characteristic determinant approach can be summarized as follows: consider a simple impurities model with a potential of

$$V(x) = \sum_{n=1}^M V_n \delta(x - x_n), \quad x_{n-1} < x_n, \quad (\text{A32})$$

where  $V_n$  is the strength of contact interaction,  $x_n$  denotes the position of the  $n$ th impurity, and  $M$  is the total numbers of scatters. The matrix elements of the  $D$ -matrix,  $\hat{D} = 1 - G_0 \hat{V}$ , for this simple contact interaction model are thus given by

$$[D(k)]_{n,n'} = \delta_{n,n'} + \frac{imV_n}{k} e^{ik|x_n - x_{n'}|}. \quad (\text{A33})$$

Let us introduce a short-hand notation

$$\mathcal{D}^{(M)} = \det [D(k)]_{M \times M}$$

to denote the determinant of the  $D$ -matrix for a system with  $M$  cells. The determinant of the  $D$ -matrix for systems with  $M$ ,  $M - 1$ , and  $M - 2$  cells, respectively, is thus related by the recursion relation

$$\mathcal{D}^{(M)} = \mathcal{A}^{(M)} \mathcal{D}^{(M-1)} - \mathcal{B}^{(M)} \mathcal{D}^{(M-2)}, \quad (\text{A34})$$

where

$$\begin{aligned} \mathcal{B}^{(M)} &= \frac{V_M}{V_{M-1}} e^{ik2(x_M - x_{M-1})}, \\ \mathcal{A}^{(M)} &= 1 + \mathcal{B}^{(M)} + \frac{iV_M}{k} (1 - e^{ik2(x_M - x_{M-1})}). \end{aligned} \quad (\text{A35})$$

The initial conditions for the recurrence relations are

$$\mathcal{D}^{(-1)} = 1, \quad \mathcal{D}^{(0)} = 1, \quad \mathcal{A}^{(1)} = 1 + \frac{imV_1}{k} = \mathcal{D}^{(1)}. \quad (\text{A36})$$

The transmission amplitude for an  $M$ -cells system is thus simply given by  $t(k) = 1/\mathcal{D}^{(M)}(k)$ . Once the transmission amplitude is given for the contact interactions model, the reflection amplitudes may be worked out simply by a matching boundary condition at the site of each scatter. The reflection and transmission amplitudes are thus related by

$$\begin{aligned} \begin{bmatrix} 1 \\ r^{(R)}(k) \end{bmatrix} &= \mathcal{M}^{(M)}(k) \begin{bmatrix} t(k) \\ 0 \end{bmatrix}, \\ \begin{bmatrix} 0 \\ t(k) \end{bmatrix} &= \mathcal{M}^{(M)}(k) \begin{bmatrix} r^{(L)}(k) \\ 1 \end{bmatrix}, \end{aligned} \quad (\text{A37})$$

where the transfer matrix for an  $M$ -cells system is given by

$$\mathcal{M}^{(M)}(k) = \prod_{n=1}^M \begin{bmatrix} 1 + \frac{imV_n}{k} & \frac{imV_n}{k} e^{-2ikx_n} \\ -\frac{imV_n}{k} e^{2ikx_n} & 1 - \frac{imV_n}{k} \end{bmatrix} \quad (\text{A38})$$

and

$$\det[\mathcal{M}^{(M)}(k)] = 1. \quad (\text{A39})$$

The transfer matrix can be parametrized in terms of transmission and reflection amplitudes by

$$\mathcal{M}^{(M)}(k) = \begin{bmatrix} \frac{1}{t(k)} & -\frac{r^{(L)}(k)}{t(k)} \\ \frac{r^{(R)}(k)}{t(k)} & t(k) - \frac{r^{(L)}(k)r^{(R)}(k)}{t(k)} \end{bmatrix}. \quad (\text{A40})$$

The left-propagating reflection amplitude,  $r^{(L)}(k)$ , can be obtained by taking advantage of the transfer-matrix relation

$$\mathcal{M}^{(M)}(k) = \mathcal{M}^{(M-1)}(k) \begin{bmatrix} 1 + \frac{imV_M}{k} & \frac{imV_M}{k} e^{-2ikx_M} \\ -\frac{imV_M}{k} e^{2ikx_M} & 1 - \frac{imV_M}{k} \end{bmatrix}, \quad (\text{A41})$$

which describes an  $M$ -cells system composed of  $(M - 1)$  cells counting from left to right plus an  $M$ th cell sitting on the right edge of the system. Using Eq. (A40) for both  $M$ -cells and  $(M - 1)$ -cells systems, the left-propagating reflection amplitude,  $r^{(L)}(k)$ , for an  $M$ -cells system is related to the determinant of the  $D$ -matrix by

$$r^{(L)}(k) = \left[ \frac{1 - \frac{\mathcal{D}^{(M-1)}(k)}{\mathcal{D}^{(M)}(k)}}{\frac{imV_M}{k}} - 1 \right] e^{-2ikx_M}. \quad (\text{A42})$$

The right-propagating reflection amplitude  $r^{(R)}(k)$  can be obtained using the same procedure by reversing the direction of operation and counting from right to left. For the  $\mathcal{PT}$ -symmetric system, left/right reflection amplitudes are related by the symmetry relation (see Ref. [40])

$$r^{(L)}(-k) = r^{(R)*}(k). \quad (\text{A43})$$

With some lengthy calculation, for the diatomic periodic  $\mathcal{PT}$ -symmetric model, we find again

$$\begin{aligned} t(k) &= \frac{1}{\det[D(k)]} = \frac{\sec(Q(2N+1)L) e^{-ik(2N+1)L}}{1 + iIm\left[\frac{e^{-ikL}}{t_0(k)}\right] \frac{\tan(Q(2N+1)L)}{\sin(QL)}}, \\ \frac{r^{(L/R)}(k)}{t(k)} &= \left[ \frac{r_0^{(L/R)}(k)}{t_0(k)} \right] \frac{\sin(Q(2N+1)L)}{\sin(QL)}, \end{aligned} \quad (\text{A44})$$

where  $Q$  is defined in Eq. (A24). The transmission and reflection amplitudes by a single cell,  $t_0(k)$  and  $r_0^{(L/R)}(k)$ , respectively, are given by

$$\begin{aligned} \frac{1}{t_0(k)} &= 1 + 2 \frac{im|V|}{k} \cos \theta + 2i \left( \frac{m|V|}{k} \right)^2 \sin(k2a) e^{ik2a}, \\ \frac{r_0^{(L/R)}(k)}{t_0(k)} &= -2 \frac{im|V|}{k} \left[ \cos(k2a \mp \theta) + \frac{m|V|}{k} \sin(k2a) \right]. \end{aligned} \quad (\text{A45})$$

The result for a general diatomic model can be found, e.g., in Refs. [48,49].

## APPENDIX B: PERIODIC $\mathcal{PT}$ -SYMMETRIC SYSTEMS

Let us also consider a periodic system

$$\left[ -\frac{1}{2m} \frac{d^2}{dx^2} + V_L(x) \right] \Psi_E^{(Q,L)}(x) = E \Psi_E^{(Q,L)}(x), \quad (\text{B1})$$

where

$$V_L(x) = \sum_{n=-\infty}^{\infty} V(x + nL)$$

is a periodic potential:  $V_L(x + nL) = V_L(x)$ . The wave function satisfies the periodic boundary condition

$$\Psi_E^{(Q,L)}(x + nL) = e^{iQnL}\Psi_E^{(Q,L)}(x), \quad (\text{B2})$$

where a superscript  $Q$  is added to label the  $Q$ -dependence of the periodic boundary condition. The stationary solutions can be found by a homogeneous LS equation for a single cell (see Refs. [70–74]),

$$\Psi_E^{(Q,L)}(x) = \int_{-\frac{L}{2}}^{\frac{L}{2}} dx' G_0^{(Q,L)}(x - x'; E) V_L(x') \Psi_E^{(Q,L)}(x'), \quad (\text{B3})$$

where the periodic Green's function of a free particle,  $G_0^{(Q,L)}(x; E)$ , is defined by

$$\begin{aligned} G_0^{(Q,L)}(x; E) &= \sum_{n=-\infty}^{\infty} G_0(x + nL; E) e^{-iQnL} \\ &= \frac{1}{L} \sum_{p=\frac{2\pi n}{L} + Q, n \in \mathbb{Z}} \frac{e^{ipx}}{E - \frac{p^2}{2m}} \\ &= -\frac{im}{k} \left[ e^{ik|x|} + \frac{\cos(kx - QL) - \cos(kx)e^{ikL}}{\cos(kL) - \cos(QL)} \right]. \end{aligned} \quad (\text{B4})$$

With the contact interactions potential in Eq. (A2), the quantization condition for eigensolutions is given by

$$\det \begin{bmatrix} 1 - V G_0^{(Q,L)}(0; E) & -V^* G_0^{(Q,L)}(2a; E) \\ -V G_0^{(Q,L)}(-2a; E) & 1 - V^* G_0^{(Q,L)}(0; E) \end{bmatrix} = 0. \quad (\text{B5})$$

Hence we again get the well-known energy-momentum dispersion relation for a periodic system (see, e.g., Refs. [48,69]),

$$\begin{aligned} \cos(QL) &= \cos(kL) + \frac{m|V|}{k} 2 \cos \theta \sin(kL) \\ &+ 2 \left( \frac{m|V|}{k} \right)^2 \sin(k2a) \sin(kL - k2a). \end{aligned} \quad (\text{B6})$$

For a periodic  $\mathcal{PT}$ -symmetric system, a generalized density of states for a single cell may be defined by

$$n_E^{(Q,L)}(x) = -\frac{1}{\pi} \text{Im}[\langle x | \hat{G}^{(Q,L)}(E) | x \rangle]. \quad (\text{B7})$$

The spectral representation of the full Green's function operator is given by (see, e.g., Appendix C in Ref. [40])

$$\hat{G}^{(Q,L)}(E) = \sum_i \frac{|\Psi_{E_i}^{(Q,L)}\rangle \langle \tilde{\Psi}_{E_i}^{(Q,L)}|}{E - E_i}, \quad (\text{B8})$$

where  $E_i = E_i(Q)$  is the  $i$ th band eigenvalue as a function of the crystal momentum  $Q$ , and the sum is over all the allowed bands.  $|\tilde{\Psi}_{E_i}^{(Q,L)}\rangle$  represents the eigenstate of adjoint Hamiltonian  $\hat{H}^\dagger$ ,

$$\hat{H}^\dagger |\tilde{\Psi}_{E_i}^{(Q,L)}\rangle = E_i |\tilde{\Psi}_{E_i}^{(Q,L)}\rangle. \quad (\text{B9})$$

The wave functions,  $|\Psi_{E_i}^{(Q,L)}\rangle$  and  $|\tilde{\Psi}_{E_i}^{(Q,L)}\rangle$ , together are biorthogonal and can be normalized in a unit cell,

$$\int_{-\frac{L}{2}}^{\frac{L}{2}} dx [\langle x | \Psi_{E_i}^{(Q,L)}\rangle \langle \tilde{\Psi}_{E_i}^{(Q,L)} | x \rangle] = 1. \quad (\text{B10})$$

Hence the integrated generalized density of states for a periodic system is now given by

$$\int_{\text{BZ}} dQ \int_{-\frac{L}{2}}^{\frac{L}{2}} dx n_E^{(Q,L)}(x) = \sum_i \int_{\text{BZ}} dQ \delta(E - E_i) = \frac{dQ}{dE}, \quad (\text{B11})$$

where integration of the crystal momentum is confined within the first Brillouin zone. We remark that the above relation is only defined in allowed bands; the density of states should be defined as zero in the gaps.

- 
- [1] N. Moiseyev, *Non-Hermitian Quantum Mechanics* (Cambridge University Press, Cambridge, 2011).
- [2] R. Landauer and T. Martin, *Rev. Mod. Phys.* **66**, 217 (1994).
- [3] V. Gasparian, M. Ortuño, G. Schön, and U. Simon, in *Handbook of Nanostructured Materials and Nanotechnology*, edited by H. S. Nalwa (Academic, Burlington, 2000), pp. 513–569.
- [4] M. Fayer and P. Fayer, *Elements of Quantum Mechanics* (Oxford University Press, Oxford, 2001).
- [5] M. Büttiker, H. Thomas, and A. Prêtre, *Z. Phys. B* **94**, 133 (1994).
- [6] P. W. Brouwer, *Phys. Rev. B* **58**, R10135 (1998).
- [7] F. Zhou, B. Spivak, and B. Altshuler, *Phys. Rev. Lett.* **82**, 608 (1999).
- [8] C. Leavens and G. Aers, *Solid State Commun.* **63**, 1101 (1987).
- [9] M. Büttiker and R. Landauer, *Phys. Scr.* **32**, 429 (1985).
- [10] M. Büttiker and R. Landauer, *IBM J. Res. Dev.* **30**, 451 (1986).
- [11] T. Martin and R. Landauer, *Phys. Rev. B* **45**, 1742 (1992).
- [12] M. Büttiker and R. Landauer, *Phys. Rev. Lett.* **49**, 1739 (1982).
- [13] R. Landauer, *Nature (London)* **365**, 692 (1993).
- [14] Y. Japha and G. Kurizki, *Phys. Rev. A* **60**, 1811 (1999).
- [15] J. Muga, S. Brouard, and R. Sala, *Phys. Lett. A* **167**, 24 (1992).
- [16] M. Büttiker, *Phys. Rev. B* **27**, 6178 (1983).
- [17] D. Sokolovski and L. M. Baskin, *Phys. Rev. A* **36**, 4604 (1987).
- [18] V. Gasparian and M. Pollak, *Phys. Rev. B* **47**, 2038 (1993).
- [19] V. Gasparian, M. Ortuño, J. Ruiz, E. Cuevas, and M. Pollak, *Phys. Rev. B* **51**, 6743 (1995).
- [20] V. Gasparian, T. Christen, and M. Büttiker, *Phys. Rev. A* **54**, 4022 (1996).
- [21] V. Gasparian, M. Ortuño, J. Ruiz, and E. Cuevas, *Phys. Rev. Lett.* **75**, 2312 (1995).
- [22] V. Gasparian, G. Schön, J. Ruiz, and M. Ortuño, *Eur. Phys. J. B* **9**, 283 (1999).
- [23] P. Balcou and L. Dutriaux, *Phys. Rev. Lett.* **78**, 851 (1997).
- [24] J. Muga, J. Palao, B. Navarro, and I. Egusquiza, *Phys. Rep.* **395**, 357 (2004).
- [25] M. Hasan, V. N. Singh, and B. P. Mandal, *Eur. Phys. J. Plus* **135**, 640 (2020).



- [26] A. Jian, F. Liu, G. Bai, B. Zhang, Y. Zhang, Q. Zhang, X. Xue, S. Sang, and X. Zhang, *Opt. Commun.* **475**, 125815 (2020).
- [27] O. Bendix, R. Fleischmann, T. Kottos, and B. Shapiro, *Phys. Rev. Lett.* **103**, 030402 (2009).
- [28] J. Schindler, A. Li, M. C. Zheng, F. M. Ellis, and T. Kottos, *Phys. Rev. A* **84**, 040101(R) (2011).
- [29] C. M. Bender, M. Gianfreda, Ş K. Özdemir, B. Peng, and L. Yang, *Phys. Rev. A* **88**, 062111 (2013).
- [30] C. M. Bender, B. K. Berntson, D. Parker, and E. Samuel, *Am. J. Phys.* **81**, 173 (2013).
- [31] C. M. Bender, M. Gianfreda, and S. P. Klevansky, *Phys. Rev. A* **90**, 022114 (2014).
- [32] N. M. Chtchelkatchev, A. A. Golubov, T. I. Baturina, and V. M. Vinokur, *Phys. Rev. Lett.* **109**, 150405 (2012).
- [33] L. Feng, R. El-Ganainy, and L. Ge, *Nat. Photon.* **11**, 752 (2017).
- [34] Z. Lin, H. Ramezani, T. Eichelkraut, T. Kottos, H. Cao, and D. N. Christodoulides, *Phys. Rev. Lett.* **106**, 213901 (2011).
- [35] L. Feng, Y.-L. Xu, W. S. Fegadolli, M.-H. Lu, J. B. Oliveira, V. R. Almeida, Y.-F. Chen, and A. Scherer, *Nat. Mater.* **12**, 108 (2013).
- [36] A. Mostafazadeh, *Phys. Rev. A* **87**, 012103 (2013).
- [37] K. G. Makris, R. El-Ganainy, D. N. Christodoulides, and Z. H. Musslimani, *Phys. Rev. Lett.* **100**, 103904 (2008).
- [38] A. Regensburger, M.-A. Miri, C. Bersch, J. Näger, G. Onishchukov, D. N. Christodoulides, and U. Peschel, *Phys. Rev. Lett.* **110**, 223902 (2013).
- [39] S. Garmon, M. Gianfreda, and N. Hatano, *Phys. Rev. A* **92**, 022125 (2015).
- [40] P. Guo and V. Gasparian, *Phys. Rev. Res.* **4**, 023083 (2022).
- [41] E. P. Wigner, *Phys. Rev.* **98**, 145 (1955).
- [42] F. T. Smith, *Phys. Rev.* **118**, 349 (1960).
- [43] M. Goldberger and K. Watson, *Collision Theory*, Dover Books on Physics (Dover, 2004).
- [44] H. Feshbach, *Ann. Phys.* **165**, 398 (1985).
- [45] D. C. Brody, *J. Phys. A* **47**, 035305 (2014).
- [46] A. Ruschhaupt, F. Delgado, and J. G. Muga, *J. Phys. A* **38**, L171 (2005).
- [47] V. Gasparian, B. Altshuler, A. Aronov, and Z. Kasamianian, *Phys. Lett. A* **132**, 201 (1988).
- [48] V. Gasparian, U. Gummich, E. Jódar, J. Ruiz, and M. Ortuño, *Phys. B: Condens. Matter* **233**, 72 (1997).
- [49] A. G. Aronov, V. M. Gasparian, and U. Gummich, *J. Phys.: Condens. Matter* **3**, 3023 (1991).
- [50] J. Korryng, *Physica* **13**, 392 (1947).
- [51] W. Kohn and N. Rostoker, *Phys. Rev.* **94**, 1111 (1954).
- [52] M. Lüscher, *Nucl. Phys. B* **354**, 531 (1991).
- [53] T. Busch, B.-G. Englert, K. Rzazewski, and M. Wilkens, *Found. Phys.* **28**, 549 (1998).
- [54] P. Guo and B. Long, *J. Phys. G* **49**, 055104 (2022).
- [55] P. Guo and V. Gasparian, *Phys. Rev. D* **103**, 094520 (2021).
- [56] P. Guo and V. Gasparian, *J. Phys. A* **55**, 265201 (2022).
- [57] P. Guo, *Phys. Rev. C* **103**, 064611 (2021).
- [58] R. El-Ganainy, K. G. Makris, M. Khajavikhan, Z. H. Musslimani, S. Rotter, and D. N. Christodoulides, *Nat. Phys.* **14**, 11 (2018).
- [59] C. M. Bender, P. E. Dorey, C. Dunning, A. Fring, D. W. Hook, H. F. Jones, S. Kuzhel, G. Lévai, and R. Tateo, *PT Symmetry* (World Scientific Europe, 2019).
- [60] M.-A. Miri and A. Alù, *Science* **363**, eaar7709 (2019).
- [61] Ş. K. Özdemir, S. Rotter, F. Nori, and L. Yang, *Nat. Mater.* **18**, 783 (2019).
- [62] C. Ferise, P. del Hougne, S. Félix, V. Pagneux, and M. Davy, *Phys. Rev. Lett.* **128**, 203904 (2022).
- [63] R. Cutkosky, P. Landshoff, D. Olive, and J. Polkinghorne, *Nucl. Phys. B* **12**, 281 (1969).
- [64] R. Eden, P. Landshoff, D. Olive, and J. Polkinghorne, *The Analytic S-Matrix* (Cambridge University Press, 2002).
- [65] A. Mostafazadeh, *Phys. Rev. Lett.* **102**, 220402 (2009).
- [66] Z. Ahmed, *J. Phys. A* **42**, 472005 (2009).
- [67] S. Longhi, *Phys. Rev. B* **80**, 165125 (2009).
- [68] P. Lloyd, *J. Phys. C* **2**, 1717 (1969).
- [69] Z. Ahmed, *Phys. Lett. A* **286**, 231 (2001).
- [70] P. Guo, *Phys. Lett. B* **804**, 135370 (2020).
- [71] P. Guo, *Phys. Rev. D* **88**, 014507 (2013).
- [72] P. Guo, J. J. Dudek, R. G. Edwards, and A. P. Szczepaniak, *Phys. Rev. D* **88**, 014501 (2013).
- [73] P. Guo, *Phys. Rev. D* **95**, 054508 (2017).
- [74] P. Guo and B. Long, *Phys. Rev. D* **101**, 094510 (2020).